



Revealing vascular abnormalities and measuring small vessel density in multiple sclerosis lesions using USPIO

Sagar Buch^a, Karthikeyan Subramanian^a, Pavan K. Jella^a, Yongsheng Chen^b, Zhen Wu^a, Kamran Shah^a, Evanthia Bernitsas^b, Yulin Ge^c, E. Mark Haacke^{a,b,*}

^a Department of Radiology, Wayne State University, Detroit, MI, USA

^b Department of Neurology, Wayne State University, Detroit, MI, USA

^c Center for Biomedical Imaging, Department of Radiology, NYU Grossman School of Medicine, New York, NY, USA

ARTICLE INFO

Keywords:

Susceptibility weighted imaging
Multiple sclerosis
Vasculature
USPIO

ABSTRACT

Background and Purpose: Multiple Sclerosis (MS) is a progressive, inflammatory, neuro-degenerative disease of the central nervous system (CNS) characterized by a wide range of histopathological features including vascular abnormalities. In this study, an ultra-small superparamagnetic iron oxide (USPIO) contrast agent, Ferumoxytol, was administered to induce an increase in susceptibility for both arteries and veins to help better reveal the cerebral microvasculature. The purpose of this work was to examine the presence of vascular abnormalities and vascular density in MS lesions using high-resolution susceptibility weighted imaging (SWI).

Methods: Six subjects with relapsing remitting MS (RRMS, age = 47.3 ± 11.8 years with 3 females and 3 males) and fourteen age-matched healthy controls were scanned at 3 T with SWI acquired before and after the infusion of Ferumoxytol. Composite data was generated by registering the FLAIR data to the high resolution SWI data in order to highlight the vascular information in MS lesions. Both the central vein sign (CVS) and, a new measure, the multiple vessel sign (MVS) were identified, along with any vascular abnormalities, in the lesions on pre- and post-contrast SWI-FLAIR fusion data. The small vessel density within the periventricular normal-appearing white matter (NAWM) and the periventricular lesions were compared for all subjects.

Results: Averaged across two independent raters, a total of 530 lesions were identified across all patients. The total number of lesions with vascularity on pre- and post-contrast data were 287 and 488, respectively. The lesions with abnormal vascular behavior were broken up into following categories: small lesions appearing only at the vessel boundary; dilated vessels within the lesions; and developmental venous angiomas. These vessel abnormalities observed within lesions increased from 55 on pre-contrast data to 153 on post-contrast data. Finally, across all the patients, the periventricular lesional vessel density was significantly higher ($p < 0.05$) than that of the periventricular NAWM.

Conclusions: By inducing a super-paramagnetic susceptibility in the blood using Ferumoxytol, the vascular abnormalities in the RRMS patients were revealed and small vessel densities were obtained. This approach has the potential to monitor the venous vasculature present in MS lesions, catalogue their characteristics and compare the vascular structures spatially to the presence of lesions. These enhanced vascular features may provide new insight into the pathophysiology of MS.

1. Introduction

Multiple Sclerosis (MS) is an inflammatory demyelinating disease characterized by a wide range of symptoms and histopathological findings (Dendrou et al., 2015). Early pathological work by Charcot and Bourneville demonstrated the involvement of the venous vasculature in MS dating back to the mid-19th century (Bourneville and Guérard,

1869; Charcot, 1868). Similarly, in the 1980 s, Adams showed evidence of vasculitis within the venous walls adjacent to active MS lesions (Adams, 1988; Adams et al., 1985; Allen, 1981). Magnetic resonance imaging (MRI) is a well-established imaging biomarker for identifying inflammatory and/or demyelinating lesions, which is critical for the clinical diagnosis of MS and evaluating drug responses (Thompson et al., 2018). With the development of susceptibility-based venography in the

* Corresponding author at: 3990 John R Street, MRI Concourse, Detroit, MI 48201, USA.

E-mail address: nmrimaging@aol.com (E.M. Haacke).

<https://doi.org/10.1016/j.nicl.2020.102525>

Received 24 August 2020; Received in revised form 26 November 2020; Accepted 1 December 2020

Available online 5 December 2020

2213-1582/Published by Elsevier Inc. This is an open access article under the CC BY-NC-ND license (<http://creativecommons.org/licenses/by-nc-nd/4.0/>).

late 1990s (Reichenbach et al., 1997), there has been a steady emphasis on the “central vein sign” or CVS hypothesis as a marker for and precursor to the development of new MS lesions (Gaitán et al., 2013; Maggi et al., 2015; Sati et al., 2016b; Tan et al., 2000). The perivascular space surrounding these veins is thought to be a privileged site for immune cells to interact with antigen-presenting cells, which can then trigger an inflammatory cascade leading to the formation of lesions around the veins (Adams, 1975; Barnett and Prineas, 2004).

Studies have demonstrated that inflammation and injury to the blood–brain barrier of post-capillary venules enables the migration of blood constituents, including erythrocytes, lymphocytes, cytokines, glial cells etc. These can contribute to the autoimmune neurodegenerative process, the onset of which could produce continuous damage eventually leading to the emergence of MS lesions. Although the current pathological understanding suggests that the veins play a major role in the formation of MS lesions, the temporal evolution of this involvement remains unclear. Vascular abnormalities can lead to collagenosis, fibrin deposition and reduction of local flow followed by oxidative stress, eventually leading to tissue necrosis. In order to study such phenomena, there is a need for a non-invasive method of imaging the microvasculature pertaining to the MS lesions. However, until recently, there has been no technique capable of imaging vessels that can visualize changes in the microvasculature, possibly before the onset of inflammation.

Previously, we developed a novel microvascular imaging approach using an ultrasmall superparamagnetic iron oxide (USPIO) contrast agent, Ferumoxytol. This method is referred to as: ‘Microvascular In-vivo Contrast Revealed Origins (MICRO)’ imaging (Buch et al., 2020; Liu et al., 2018; Shen et al., 2020). MICRO imaging, which takes advantage of the susceptibility weighted imaging (SWI) sequence, has shown potential in studying small vessels that previously could only be seen in cadaver brain studies (Buch et al., 2020). By inducing a non-zero susceptibility into the blood, both small arteries and veins can be seen not only in healthy tissue but also in MS plaques. With sufficiently high resolution, cerebral microvasculature can now be seen *in vivo* at 3 T (Buch et al., 2020). This approach has the potential to monitor the venous vasculature present in MS lesions and compare the vascular structures spatially to the presence of white matter hyperintensities (WMH) of MS lesions.

In this work, we have studied the application of high-resolution MICRO imaging in enhancing the vascular contrast and mapping the microvascular nature of MS lesions. The T_1 -enhancement and T_2^* -related signal loss, due to the presence of Ferumoxytol, were compared in terms of improving the visibility of the sub-voxel vessels. We have employed a combination of the co-registered SWI and FLAIR data to highlight the vascular information inside the MS lesions (Haacke et al., 2020). In addition, several unique venous vascular anomalies were identified and characterized using the composite SWI-FLAIR data. The periventricular white matter and lesional vessel density were obtained from the MICRO SWI data by employing a lesion segmentation approach and a novel vessel mapping method.

2. Methods

2.1. Subjects

Data were acquired with local institutional review board approval at Wayne State University (Detroit, MI, USA) and all subjects signed an informed consent form. Six subjects with relapsing remitting MS (RRMS, age = 47.3 ± 11.8 , from 32 to 62 years old, 3 women) were included in the study. Fourteen age-matched healthy controls (HCs) were recruited to see if any similar vascular abnormalities seen in the MS patients were present. FLAIR data was acquired for seven healthy controls.

Inclusion criteria for patients were as follows: at least 18 years of age, able to understand and sign the consent form, a confirmed diagnosis of RRMS according to the revised McDonald criteria (Thompson et al., 2018), in good health with the exception of MS, and neurologically

Table 1

MRI sequence parameters across all subjects. * Five healthy controls were acquired with a FA of 12° for the SWI sequence. ** SWI data for these subjects were reconstructed from the anisotropic in-plane resolution of $0.22 \times 0.44 \text{ mm}^2$ to $0.22 \times 0.22 \text{ mm}^2$. *** For patient 1, the time of acquisition was 5:14, due to a lower oversampling utilized (25% instead of 33% for the remaining subjects).

Parameters	MS patients 1–3			MS patients 4–6 and All healthy controls		
	T1W	FLAIR	SWI	T1W	FLAIR	SWI
TR (ms)	1400	6000	30	1500	6000	27
TE(s) (ms)	3.4	397	15	3.4	395	7.5, 15
FA ($^\circ$)	9	120	12	9	120	12*, 15
TI (ms)	–	2200	–	–	2200	–
In-plane resolution (mm^2)	0.47	0.75×0.75	0.23×0.23	0.44	0.88×0.88	$0.22 \times 0.44^{**}$
Slice thickness (mm)	1.5	1.5	1.5	1	1	1
Bandwidth (Hz/pxl)	181	679	80	181	514	181
GRAPPA acceleration	2	2	2	2	2	2
Acquisition time (mins:secs)	3:45	5:32***	11:01	4:20	5:20	10:36
Ferumoxytol dose (mg/kg)	3			4		

stable with no evident relapse or corticosteroid treatment in the last 30 days prior to the screening visit (expanded disability status scale (EDSS) range of 0–5, and disease duration range of 2–18 years). Exclusion criteria for patients were as follows: pregnant or nursing, MRI contraindicated, a history of hypertension or hypotension, previous vascular intervention or major illness, a priori known neurological disorder (other than MS), history of substance abuse, progressive MS diagnosis, incidents of seizure or unexplained blackouts within six months of screening, known sensitivity or allergy to iron based contrast agents or any significant brain abnormality other than MS.

2.2. MR imaging

All subjects were scanned on a 3 T MRI scanner (Verio, Siemens Healthineers, Erlangen, Germany) with a 32-channel head coil. The imaging protocol included: axial T1 weighted magnetization prepared rapid gradient echo (MPRAGE), axial 3D FLAIR and axial 3D gradient echo SWI sequences. The SWI sequence, which was used to acquire the MICRO data, was adapted by correcting the echo shift in each individual coil before phase combination (Chen et al., 2018). The first echo time (TE) was flow compensated in slice/read directions, whereas the second TE was not flow compensated. The SWI and T1 MPRAGE sequences were collected before and after the administration of Ferumoxytol (Feraheme, AMAG Pharmaceuticals, Inc. Waltham, MA, USA). Detailed imaging parameters across all subjects are listed in Table 1.

For all subjects, the phase and magnitude SWI data from the common TE of 15 ms were used for all SWI-related analyses. In order to demonstrate the advantage of acquiring high resolution data, the acquired data with $0.22 \times 0.22 \times 1 \text{ mm}^3$ voxel resolution (reconstructed from the resolution of $0.22 \times 0.44 \times 1 \text{ mm}^3$ data) was collapsed in k-space to lower resolutions of $0.22 \times 0.22 \times 1.5 \text{ mm}^3$, $0.44 \times 0.44 \times 1.5 \text{ mm}^3$, $0.22 \times 0.22 \times 2 \text{ mm}^3$ and $0.44 \times 0.44 \times 2 \text{ mm}^3$. The resultant SWI data at each resolution were compared to understand the detectability of the sub-voxel vessels. Additionally, a separate single-TE SWI data was acquired for one of the healthy controls using the same imaging protocol as the other healthy control data, as shown in Table 1, with the exception of using a conventionally long TE of 22.5 ms (instead of 15 ms) and an acceleration factor of 3 (instead of 2). This data was acquired to compare the vessel contrast between conventional non-contrast SWI (TE = 22.5 ms) and the post-contrast SWI data (TE = 15 ms).

2.3. Data processing

The SWI images were generated by homodyne high-pass filtering (filter size = 96×96) the phase images. A phase mask was then generated from the high-pass filtered phase data, which was multiplied into the original magnitude images four times (Haacke et al., 2004). For each subject, all the post-contrast original magnitude, SWI and FLAIR data as well as the pre- and post-contrast T1 data were registered to the pre-contrast long TE (15 ms) magnitude data of the dual-echo SWI acquisition. The image registration was performed using the statistical parametric mapping (SPM) package (SPM12, Wellcome Centre for Human Neuroimaging, University College London, London, UK) in MATLAB (MathWorks, Inc., Natick, MA, USA) by using normalized mutual information as the cost function and a 4th degree spline for interpolation (Ashburner and Friston, 1997; Collignon et al., 1995; Studholme et al., 1999). The transform parameters obtained from magnitude data registration were then applied to the SWI data. In order to highlight the vascular information within the WMHs, the registered FLAIR data was multiplied with the registered pre- and post-contrast SWI data to generate the pre- and post-contrast SWI-FLAIR data, respectively (Haacke et al., 2020). The registered post-contrast T1-MPRAGE data was divided by the pre-contrast T1-MPRAGE data to obtain a map of T1-enhancement within the blood vessels ($T1_b$). This $T1_b$ data was then compared with the SWI-FLAIR data in the region of a lesion.

The CVS, defined as the presence of a single dominant vessel in the center of the lesion, was identified using SWI-FLAIR data. Since not all vessels are centrally located in the MS lesions but sometimes appear throughout or on the edges of the lesions, we defined a new term called the multiple vessel sign (MVS) to distinguish a broader distribution of veins inside the lesions. Each lesion was then evaluated for the presence of a CVS, MVS, an abnormality (as covered in section 2.5) or no vessels at all on both the pre- and post-contrast SWI-FLAIR data.

In order to obtain the quantitative susceptibility mapping (QSM) results from the pre-contrast SWI, the phase data was unwrapped using the 3D best-path method (Abdul-Rahman et al., 2007). Sophisticated harmonic artifact reduction for phase data (SHARP) method (kernel size = 6 voxels) (Schweser et al., 2011) was used to estimate the background field and remove it from the unwrapped phase. The truncated k-space inverse filter approach with an iterative geometric constraint was applied to the resultant phase in order to generate the susceptibility maps (regularization threshold = 0.15) (Tang et al., 2013).

2.4. Inter-rater analysis

The lesion identification process on FLAIR data was reviewed in consensus by a radiologist (Zhen Wu) and two raters or field experts (Sagar Buch = SB or rater 1 ab and Karthikeyan Subramanian = KS or rater 2) on one MS patient. This was followed by the blinded lesion detection on the FLAIR data by the two raters (SB, KS) for all subjects. For vascular signs, the two raters (SB, KS) first evaluated one subject individually to study the CVS, MVS and abnormal cases. Consequently, they shared their findings and worked in consensus to define each vascular sign category, including CVS and MVS, by examining a few randomized lesions. Each MS patient data were then evaluated individually by the same two raters.

All the vascular signs (CVS, MVS and the abnormalities) inside the MS lesions were identified by evaluating the SWI-FLAIR data, along with the original SWI and FLAIR images. These images (SWI, FLAIR and SWI-FLAIR) were zoomed by a factor of 2, when needed, in the area of the lesion to confirm the presence of a vascular sign. This step was especially useful for the smaller lesions that are associated with smaller vessels, which can be difficult to view on the original, zoomed-out images. Similarly, the SWI, FLAIR and SWI-FLAIR data from the healthy controls were reviewed to ascertain if any similar abnormalities occurred in HCs. All the visual image analyses, including the manual detection process,

was performed on SPIN-Research software (SpinTech Inc., Bingham Farms, MI, USA).

2.5. Classifying vascular abnormalities

The vascular abnormalities were classified based on the following criteria: i) differences in the vessel size within and outside the MS lesion; ii) size of the lesion with respect to the vessels; and iii) the presence of a fully-developed venous angioma (a spoke-like conglomeration of veins within the lesion) or hint of a developing angioma, comprised of smaller vessels, with the vascular junction located in the center of a lesion. Based on these criteria, the anomalies were classified into following five sub-types:

1) *Small ovoid WMHs*: Although an MS lesion usually appears along almost the entire length of the vessels (the usual CVS), in some cases there were small local regions (<3 mm in length) of WMHs with no vascularity on non-contrast data, which are generally not considered during MS lesion classification (Sati et al., 2016a). However, these small WMHs also appeared to be located surrounding the vessel wall of the smaller vessels on the post-contrast SWI-FLAIR data. The presence of these lesions also supports the work done by Fog, who stated that MS lesions typically developed around small vessels (Fog, 1964). Care was taken to avoid the confusion between this category and CVS by assessing the length of the long axis for a given lesion.

2) *Dilated vessels*: With the help of the post-contrast SWI and SWI-FLAIR data, it was possible to detect the local change in diameter for the vessels. The lesions that contain vessels exhibiting a change in diameter were placed into this category. These anomalies are different than the lesion containing CVS on the basis that there is an intra-lesional abrupt change in diameter of the vessel. It has been shown that in stroke and restricted retrograde venous hypertension, deep medullary veins could dilate or appear dilated in SWI due to the increased levels of deoxyhemoglobin (Li et al., 2013). Similar to Schelling's work (Schelling, 1986), Allen noticed wide vascular beds around veins and central widening of the venous tree; these changes testify to an intermittent increase in cerebral pressure (Allen, 1981). In order to confirm this abrupt diameter change, both the original and minimum intensity projections (mIP) of SWI data, with effective slickness of 3 mm and 5 mm, were examined to increase the overall visualization of the vessel in and outside the lesion.

3) *Perpendicular vessel development*: A perpendicular vessel formation to the vascular drainage or supply pathway was categorized as a separate anomaly. This specific formation may suggest vascular remodeling (anastomosis) due to local obstructed flow caused by venous collagenosis or endothelial dysfunction (Caprio et al., 2016; Poser, 1986; Yanagisawa et al., 1988).

4) *Lesion centric developmental venous anomalies (DVA)*: DVAs are known cerebro-vascular malformations that involve an irregular arrangement of small veins converging centripetally into a large draining vein (Lee et al., 1996; Saba, 1998).

5) *Micro DVAs*: Similar to the fourth category, this classification of anomalies is also related to lesion-centric angiomas but with fewer (~3–4 vessels), much smaller (1 voxel-wide visibility) veins that show a hint of an irregular, spoke-like vascular pattern. These micro-DVAs were usually only visible on the post-contrast SWI-FLAIR data.

2.6. Obtaining periventricular vessel density (PVD)

In order to evaluate a change in PVD, a special map of cerebral vasculature was constructed using the MICRO data. An initial vessel map was generated by subtracting the post-contrast SWI data from the original magnitude of the pre-contrast data and was linearly interpolated in 2D by a factor of 2×2 to improve small vessel detection during the vessel tracking process. To improve the contrast of the vessels and suppress any $T2^*$ -related signal in the surrounding tissues, the Frangi vesselness filter (Descoteaux et al., 2008; Frangi et al., 1998) was

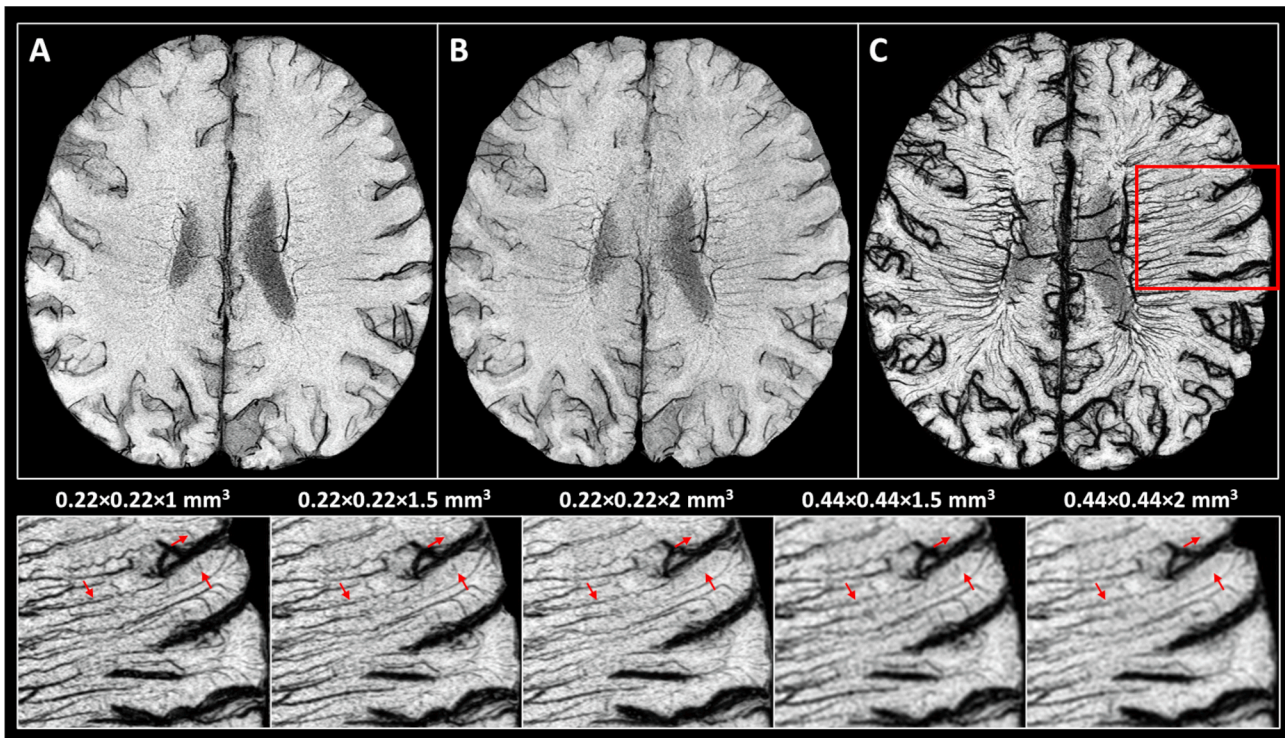


Fig. 1. Advantage of high resolution SWI in the presence of Ferumoxytol to reveal the cerebral microvasculature. For a healthy volunteer, the pre-contrast SWI data were acquired with a TE of 15 ms for the MICRO protocol (A) and with a conventional TE of 22.5 ms (B). The post-contrast (4 mg/kg concentration of Ferumoxytol) SWI data (C) shows a dramatic improvement in visualizing the cerebral vasculature as compared to both the pre-contrast SWI data. The images (A) to (C) were acquired with a resolution of $0.22 \times 0.22 \times 1 \text{ mm}^3$ (reconstructed in k-space from $0.22 \times 0.44 \times 1 \text{ mm}^3$ data) and minimum intensity projected (mIP) over 6 slices. The effect of the voxel size on the small vessel contrast was evaluated as shown in the bottom row of zoomed insets (with the region identified by the red box in (C)). The resolution of the post-contrast data (C) was reduced by cropping k-space elements to obtain the lower voxel resolutions (in mm^3) of $0.22 \times 0.22 \times 1.5$, $0.22 \times 0.22 \times 2$, $0.44 \times 0.44 \times 1.5$ and $0.44 \times 0.44 \times 2$. The data with slice thickness of 1 mm, 1.5 mm and 2 mm in the bottom row were mIP over 6, 4 and 3 slices, respectively, to produce an effective slice thickness of 6 mm. The higher in-plane and through plane resolution on Ferumoxytol-enhanced SWI helps in revealing the underlying vessels (red arrows). (For interpretation of the references to colour in this figure legend, the reader is referred to the web version of this article.)

applied to a linearly interpolated (interpolation factor = 2×2) post-contrast SWI data. The vesselness measures were computed by setting the α , β and γ parameters in Eq. 13 of (Frangi et al., 1998) to 0.5, 0.5 and half of the maximum Hessian norm as suggested in their work. At each voxel, the vesselness was computed using 10 log scale increments between 0 and 10 voxels (assuming that maximum radius of a vessel is 10 voxels) and the maximum vesselness response along with its scale were selected (Descoteaux et al., 2008). A threshold of 0.015 was used to reduce the noise in the vesselness images.

The resultant vesselness measures and the initial vessel map, both defined above, were averaged to obtain an improved vessel map. This step suppresses the T_2^* -related signal and noisy pixels that were picked up by the vesselness measure. For vessel tracking, the pixels in $5 \times 5 \times 5$ neighborhood were iteratively evaluated from the seed region by selecting only the pixels that were above the mean $- 2\sigma$, where σ is the standard deviation within the seed region and was updated by including the newly selected pixels after each iteration. The structural similarity index (SSIM) between the tracked results of the current and previous iterations was obtained; and was used to end the iterative process at $\text{SSIM} > 0.9999$ (Zhou Wang et al., 2004). All the major veins that were visible on the pre-contrast MICRO data were suppressed using the venous mask generated from the QSM results using a threshold of 250 ppb.

3D periventricular WM masks were obtained through the WM parcellation matrix generated using Freesurfer (version 4.5.0, <http://surfer.nmr.mgh.harvard.edu/>) (Collins et al., 1994; Fischl et al., 2004, 2002). Three equal sub-divisions, along the antero-posterior length of this periventricular WM mask, were produced and were labeled as anterior, middle and posterior periventricular WM. For each sub-division, care was taken to discard the pixels representing the basal ganglia structures

and cerebro-spinal fluid that were incorrectly included into the periventricular WM masks. The periventricular lesions were segmented in 3D using the lesion prediction algorithm implemented in SPM's lesion segmentation toolbox (Schmidt, 2017; Schmidt et al., 2012). The PVD, defined by (number of vessel-containing voxels) / (total number of voxels), was obtained for the normal-appearing WM (NAWM) masks and lesion masks for the three periventricular sub-divisions from each MS patient. Similarly, the PVD was obtained for the periventricular WM from each healthy subject. The ratio of lesion-to-NAWM volume was also obtained as a reference in each sub-division and was compared with the difference in PVDs of lesions and NAWM.

2.7. Statistical analysis

The intra-class correlation coefficient (ICC), specifically ICC(A,1), was used to determine the inter-rater agreement the number of CVS, MVS, total vascular lesions (CVS, MVS or other vascular abnormalities) and number of lesions identified on FLAIR (McGraw and Wong, 1996; Shrout and Fleiss, 1979). ICC scores below 0.4 were considered as poor agreement, 0.4–0.6 as reasonable, 0.6–0.7 as good, and 0.7–1 as excellent (Bartko, 1991; Cicchetti, 1994). The pre- and post-contrast SWI-FLAIR data were compared using a paired *t*-test to confirm that the visibility of vascular anomalies increased consistently for all subjects (significance level of 95%). The number of MVS, CVS and the percentage detectability of vascular anomalies were obtained for each subject. The mean \pm inter-subject variability of the percentage detectability was obtained from both the pre- and post-contrast SWI-FLAIR datasets. The percentage detectability was calculated as the number of lesions with CVS, MVS or vascular anomalies on SWI-FLAIR data divided by the total

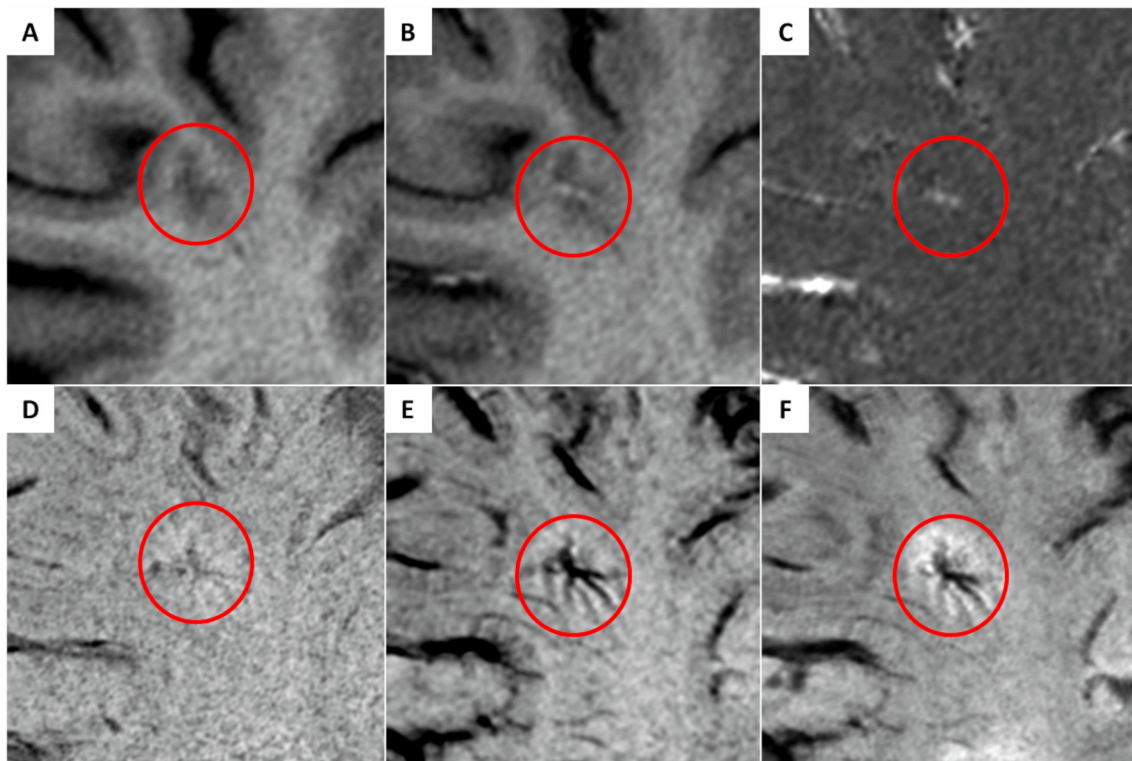


Fig. 2. Angioma visualized in (A) pre-contrast T1W data, (B) post-contrast T1W data, (C) T1_b data, (D) pre-contrast SWI, (E) post-contrast SWI (4 mg/kg dose) and (F) SWI-FLAIR data for an MS patient. The T1_b data, which displays T1-enhancement of Ferumoxytol, only partially highlights the main draining vein of the angioma. Although there is a hint of the spoke-like vessels on the pre-contrast SWI data (suggesting that the angioma is draining into a major vein), the angioma is seen significantly better on the post-contrast SWI data. The SWI-FLAIR confirms the lesion-centric nature of the venous angioma and shows that the extent of the vascular abnormality essentially defines the extent of the lesion as well.

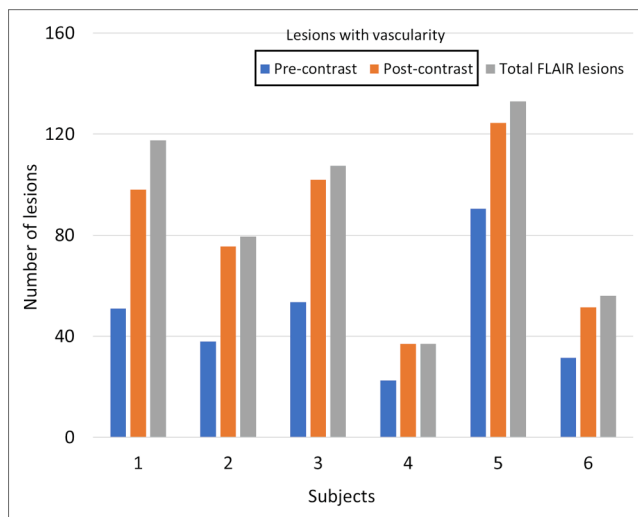


Fig. 3. Number of lesions with vascularity (CVS, MVS or any of the vascular anomalies) observed for each subject on pre- and post-contrast SWI-FLAIR data were compared with all the lesions detected on the FLAIR data. All the values were averaged across the two independent raters. The post-contrast SWI-FLAIR significantly improved the detectability of the vasculature within the lesions. The number of CVS, MVS and vascular abnormalities for each subject and each rater on both pre- and post-contrast SWI-FLAIR data are listed in Table 2.

number of MS lesions on FLAIR data. The estimated PVD of the lesions and NAWM were compared for each subject using the paired *t*-test (significance level of 95%). Spearman's correlation coefficient was used to test the correlation for the ratio of lesion-to-NAWM volume with the

difference in PVDs of lesions and NAWM ($p < 0.05$ was considered to be statistically significant).

3. Results

Fig. 1 shows the improvement in delineating the periventricular vessels using high in-plane and high through-plane resolution with MICRO imaging. The post-contrast SWI data (TE = 15 ms, Fig. 1C) shows a dramatic improvement in revealing the vasculature as compared to both the pre-contrast SWI data (TEs = 15 ms and 22.5 ms or Fig. 1A and 1B, respectively). However, as the resolution decreases, the sharpness of all vessels decreases and smaller vessels disappear. For example, the small vessels, identified by the red arrows, appears clearly on the in-plane resolutions of $0.22 \times 0.22 \text{ mm}^2$ as long as the slice thickness does not exceed 1.5 mm. Fig. 2 shows the visualization of a venous angioma in magnitude and T1W data before and after contrast for an MS patient. Ferumoxytol makes the angioma and the tiny vasculature associated with it more clearly visible on the SWI-FLAIR data; whereas the T1W post-contrast image was only able to show part of a single large, possibly dilated vessel (Fig. 2B, C). Fig. 3 shows the number of vascular signs (CVS, MVS and vascular abnormalities) observed in the MS lesions on pre- and post-contrast SWI-FLAIR data, along with the total number of lesions identified on FLAIR data, for each subject, averaged across the two independent raters. Agreement among the two raters in the detecting the CVS (ICC > 0.95), MVS (ICC > 0.8), all the lesion-centric vascular signs, including the CVS, MVS and vascular abnormalities, (ICC > 0.9) on SWI-FLAIR data and the number of lesions (ICC > 0.95) on FLAIR data was excellent. The individual ratings, on pre- and post-contrast SWI-FLAIR data, are listed in Table 2; along with the individual EDSS scores and disease durations. The presence of Ferumoxytol increased the visibility of the vessels significantly ($p < 0.05$) compared to the pre-contrast data for each MS patient. The mean \pm inter-subject

Table 2

Clinical characteristics and the vascular signs on post-contrast SWI-FLAIR data for each subject from two raters. The detected vascularities are shown here in the form of: Rater 1 value (Rater 2 value). DVA = developmental venous anomaly; EDSS = expanded disability status scale; CVS = central vein sign; MVS = multiple vessel sign.

Patient number	EDSS	Disease duration		Vascular anomalies				CVS	MVS	
				Small ovoid WMHs	Dilated	Perpendicular	Macro DVA			Partial/micro DVA
1	3.5	6	Pre	11 (9)	0 (1)	1 (1)	1 (1)	0 (0)	29 (27)	7 (14)
			Post	37 (41)	0 (1)	1 (1)	1 (1)	0 (0)	31 (35)	24 (22)
2	5	2	Pre	4 (5)	1 (1)	0 (0)	0 (0)	0 (0)	22 (25)	8 (11)
			Post	17 (16)	1 (1)	0 (0)	0 (0)	2 (1)	36 (34)	19 (24)
3	0	3	Pre	9 (7)	1 (1)	1 (0)	1 (1)	0 (0)	28 (24)	17 (18)
			Post	39 (35)	1 (1)	1 (1)	1 (1)	2 (2)	32 (34)	28 (26)
4	7	18	Pre	5 (5)	0 (1)	0 (0)	0 (0)	0 (0)	13 (12)	4 (6)
			Post	9 (8)	1 (1)	0 (0)	0 (0)	0 (0)	13 (14)	13 (16)
5	0	13	Pre	15 (17)	0 (0)	0 (0)	1 (0)	0 (0)	52 (53)	17 (26)
			Post	24 (36)	0 (0)	1 (1)	0 (0)	0 (0)	58 (60)	29 (40)
6	2.5	14	Pre	6 (4)	0 (1)	0 (0)	0 (0)	0 (0)	19 (20)	5 (8)
			Post	9 (9)	0 (1)	0 (0)	0 (0)	0 (0)	25 (23)	17 (19)

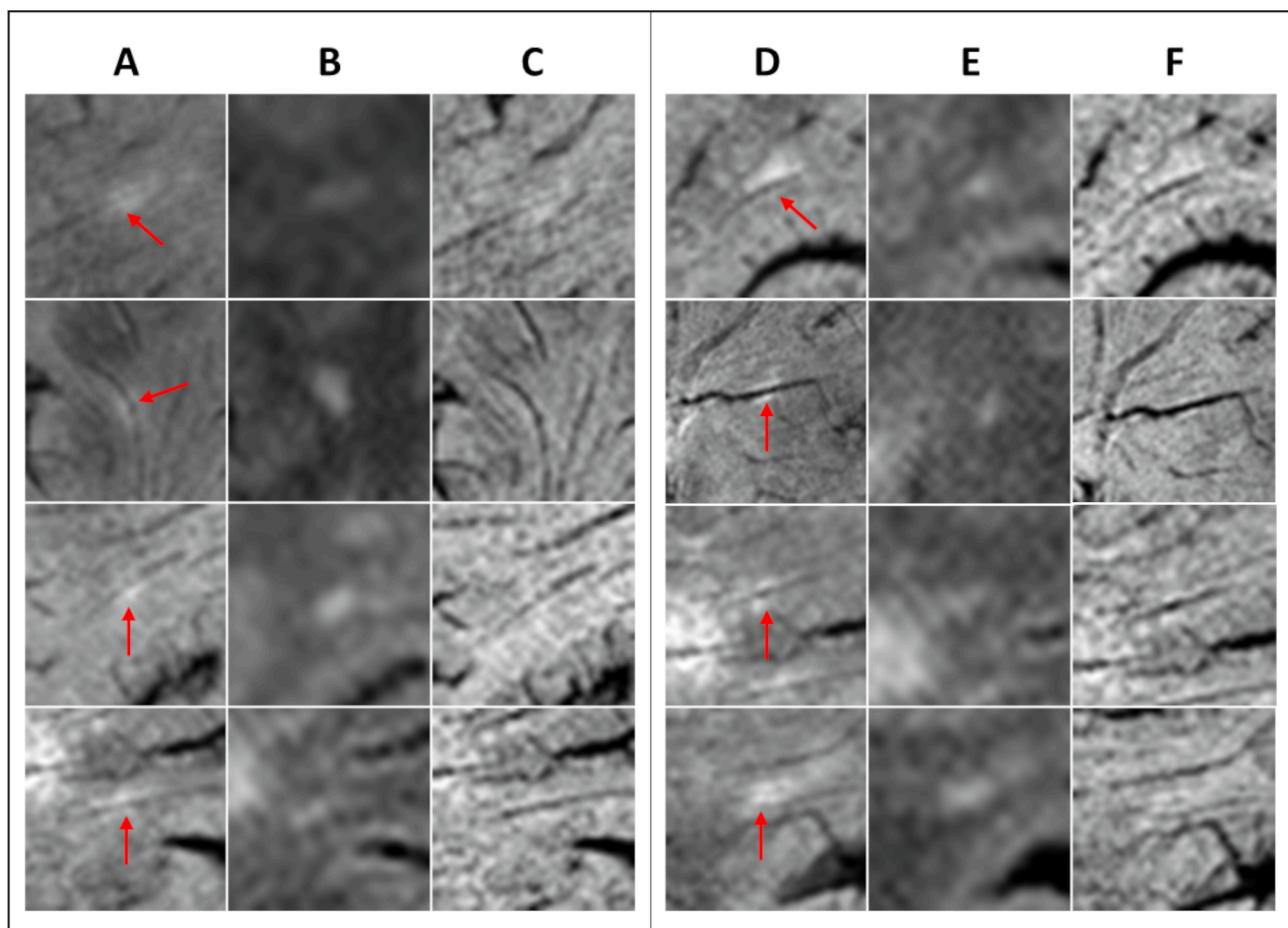


Fig. 4. Eight cases of small ovoid WMHs surrounding a vessel for a possible developing lesion (red arrows). The SWI-FLAIR data (A and D) offers better subtle lesion detection associated with the veins than the FLAIR-only data (B and E) or SWI-only data (C and F). (For interpretation of the references to colour in this figure legend, the reader is referred to the web version of this article.)

variability of the percent detectability on pre-contrast was $54.3\% \pm 9.1\%$, which improved to $93.7\% \pm 5.5\%$ post-contrast. Across the raters, i.e. rater 1 (rater 2), for the 521 (540) lesions detected on FLAIR data, the total number of lesions with a vascular sign increased from 275 (299) lesions on the pre-contrast data to 475 (505) lesions on the post-contrast SWI-FLAIR data; which is an increase in visibility by factor of roughly 1.7.

Figs. 4-7 demonstrate the different types of unique vascular anomalies. Selected cases for small ovoid WMHs are displayed in Fig. 4. The lesions surrounding the vessels are smaller in size and only encapsulate

the veins partially along one or both sides of the vessel. Fig. 5 shows the cases of dilated vessels within the lesion, where the intra-lesional vessel diameter is visibly larger than the perilesional vessel diameter, as confirmed on the SWI mIPs with effective thickness of 3 mm and 5 mm. In this figure, the case on the second row was rejected after examining the mIPs due to the visible confluence of vessels at the location of abrupt decrease in vessel diameter. The perpendicular vessel development was usually observed at the boundary of the corona radiata (Fig. 6) specifically where there is a reduction in intensity from medial-to-lateral direction in the WM (yellow traces in Fig. 6A and 6F). Two definite cases of

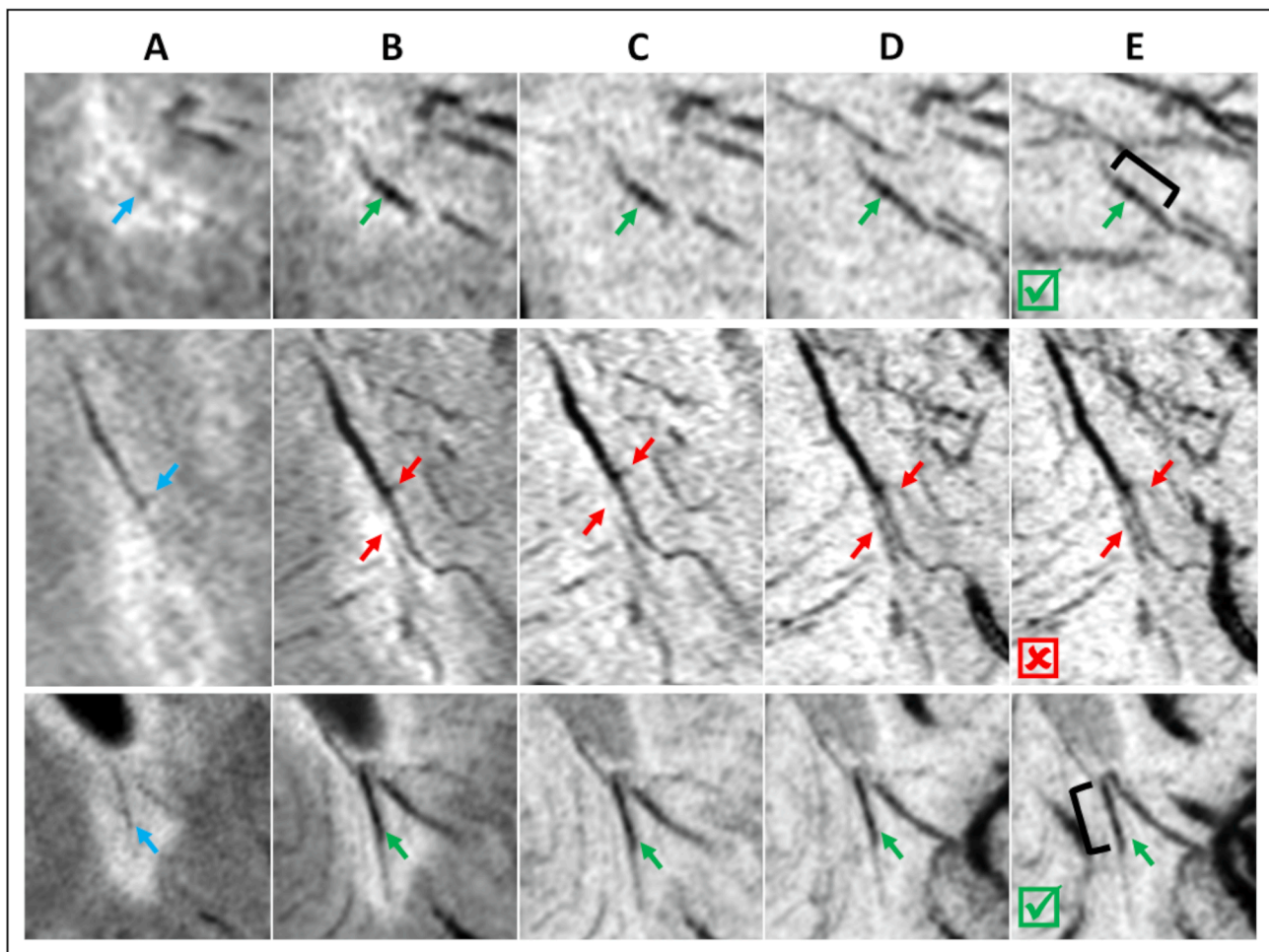


Fig. 5. Dilated vasculature associated with the MS lesions as seen on the pre-contrast (A) and post-contrast (B) SWI-FLAIR data. The vessel detection on the pre-contrast SWI confirm the venous origin of the dilated vessel candidates (blue arrows). On the other hand, the post-contrast SWI (C), minimum intensity projections (mIPs) of the original SWI with effective slice thickness of 3 mm (D) and 5 mm (E) were carefully examined to determine the vessel dilation. The cases with green check marks were considered as dilated vessels (green arrows and black brackets), whereas the red cross identifies the case with a false positive in terms of vessel dilation within a lesion due to the confluence of smaller blood vessels (red arrows). (For interpretation of the references to colour in this figure legend, the reader is referred to the web version of this article.)

venous angiomas are shown in Fig. 7A and 7F displaying an irregular centripetal collection of vessels within the lesion that drain into a major vein. In these cases, the extent of the DVAs as seen on SWI-FLAIR data predicts the region of inflammation. On the other hand, the cases that displayed a hint of such arrangement through sub-voxel vessels were also observed, as seen in Fig. 7K and 7P. These might later develop into a fully-formed angioma. The occurrence of all the anomalies for each patient as detected by the two raters are also listed in Table 2. The patient data shown in Figs. 2, 6 and 7 were taken from the scan protocol for patients 1–3, whereas the data shown in Figs. 4 and 5 were taken partly from both scanning protocols. The pre-contrast SWI-FLAIR data were used to confirm the venous origin of the abnormalities in Figs. 5, 6 and 7, as highlighted by the blue arrows.

Out of all the healthy controls that had FLAIR data ($n = 7$), three controls showed WMHs (total number of non-MS WMHs = 7) on the FLAIR data. All the non-MS WMHs that were studied in this work (four example cases are shown in Fig. 8) showed a vascular sign associated with them. Four out of these seven non-MS WMHs were classified under the ‘small ovoid WMHs’ category, two were classified under CVS and the remaining one was classified as an MVS.

An example of mapping the periventricular vasculature is shown in Fig. 9. The periventricular WM was divided into three sections (Fig. 9A). The major veins were discarded from the vessel maps by using the pre-contrast QSM data (Fig. 9B). The improved vessel maps were able to

suppress the surrounding tissues and enhance the vessels (Fig. 9C). The final vessel tracking results (Fig. 9E) was able to segment most of the sub-voxel vessels that were visible on the post-contrast SWI data (Fig. 9D). Similarly, an example of a periventricular WM mask (obtained using the WM parcellation) and lesion mask (yellow arrows), obtained using the lesion prediction algorithm, are demonstrated in Fig. 10A and 10B, respectively. The NAWM (blue arrows) was defined by the region outside the lesions and within the periventricular WM mask. Across all the patients and for each periventricular sub-division, the lesional PVD was significantly higher ($p < 0.05$) than the periventricular NAWM PVD, as shown in Fig. 11. Furthermore, the difference between lesional PVD and NAWM PVD was not in correlation ($p > 0.05$) with the lesion-to-NAWM ratio, suggesting that the periventricular WM, lesional masks did not interfere with the difference in the PVDs. On the other hand, the NAWM PVD estimated from the patients were within the range of WM PVD in the healthy controls (Fig. 11D).

4. Discussion and Conclusions

This study demonstrated that MICRO imaging can reveal the microvasculature associated with MS lesions that are otherwise invisible to conventional imaging, as shown in Fig. 1. This has led to the findings that there are a number of venous abnormalities in MS lesions, specifically there are five different signs indicative of changes at the small

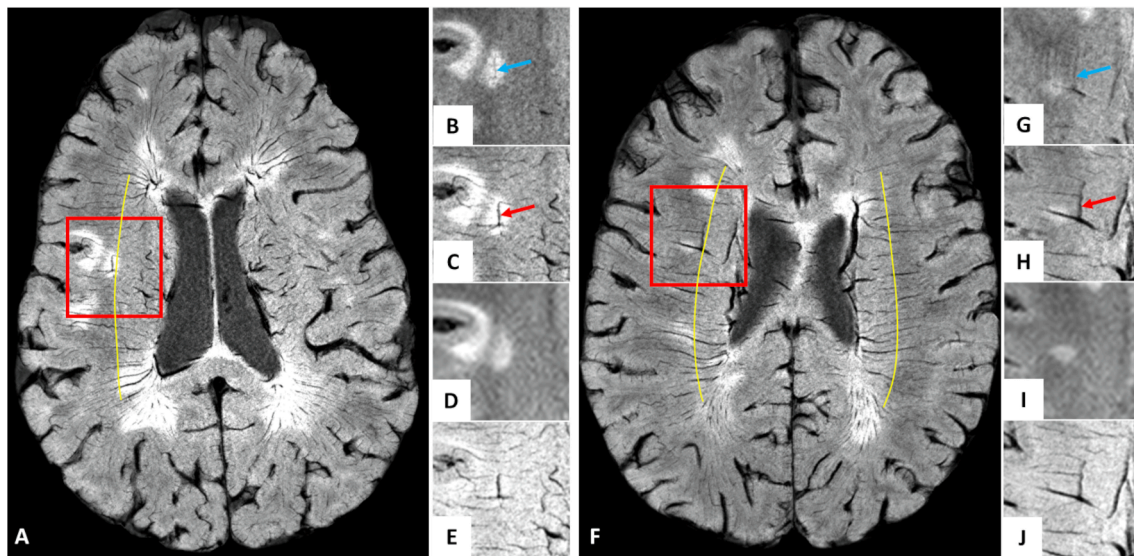


Fig. 6. Lesion development surrounding the perpendicular vessels as seen on the SWI-FLAIR data of two selected MS patients (A and F), along with the zoomed insets of the pre-contrast SWI-FLAIR (B and G), post-contrast SWI-FLAIR (C and H), original FLAIR (D and I) and original SWI data (E and J). These perpendicular veins abet to, what appears to be, the corona radiata (yellow traces); and were visible on both pre-contrast (blue arrows) and post-contrast data (red arrows). (For interpretation of the references to colour in this figure legend, the reader is referred to the web version of this article.)

vessel level. Some of these abnormalities were clearly discernible (e.g., the DVAs and perpendicular vessels), whereas the others were only classified as one of the categories after careful examination (e.g., dilated vessels and small ovoid WMHs). Similar to previous work (Grabner et al., 2011; Sati et al., 2012), the combination of SWI and FLAIR data makes it possible to obtain a single image for the assessment of the venous vasculature in relation to the WMHs and provides much better delineation of the sub-voxel vasculature than T1_ρ data (Fig. 2). However, the method introduced by Grabner et al. requires a fusion of FLAIR data acquired at 3 T with the phase mask of the SWI data acquired at 7 T, whereas a very similar approach proposed in this paper uses only 3 T datasets (Grabner et al., 2011). In order to compensate for the increased sensitivity of the vasculature at 7 T shown by Grabner et al., we take advantage of Ferumoxytol administration to increase the detectability and rendering of the small vessels at 3 T. Sati et al. have also utilized the susceptibility-weighted data, acquired using a T₂*-weighted segmented echo planar imaging (SEPI) sequence, to enhance the FLAIR data (Sati et al., 2012). The drawback of their method is the ability to acquire only one TE, which can limit the application of the sequence based on the susceptibility of the tissue-of-interest. Another drawback with the SEPI approach is that both arterial and venous signals will be hypointense, whereas the GRE-based SWI acquisition that was used in this paper has bright arterial signal on the first TE due to the flow compensation gradients. This natural separation of arterial and venous signals is essential to identify the CVS for the WMHs on the pre-contrast data. Furthermore, studies have shown that SWI is more sensitive than the T₂*-weighted images in detecting hemorrhagic lesions (Tong et al., 2004, 2003; Wycliffe et al., 2004), cavernous malformations (Sparacia et al., 2016), microbleeds (Cheng et al., 2013; Haacke et al., 2007), small venous network (Chavhan et al., 2009; Lee et al., 1999; Mittal et al., 2009; Reichenbach et al., 2001).

A number of papers have proposed using a 40% or 50% rule to distinguish MS lesions with CVS from the WMHs in other neurological diseases (Mistry et al., 2016; Sati et al., 2016b; Tallantyre et al., 2011). This specificity for the pathogenesis of vascular network pertaining to MS lesions could be further reduced on non-USPIO data if the venous oxygenation level is increased in MS (Ge et al., 2012, 2009). However, MICRO imaging showed a much greater number of lesions with a vascular sign increasing from 54% to 93%, in the presence of Ferumoxytol, over all subjects, along with the potential of revealing several

types of vascular abnormalities that are almost invisible on non-USPIO data. Although the proposed process requires administration of a contrast agent, it significantly improves the sensitivity of detecting the vascularity associated with the WMHs. Consequently, the diagnostic criteria could be revisited due to this increased sensitivity of the microvasculature, along with the severity of MS-related symptoms. However, this will require a study that involves a large number of MS patients and the ability to differentiate between the venous and arterial components within the lesions; which is lacking in this pilot study.

The SWI-FLAIR data shows clear evidence of small, potentially active MS lesions developing along the vessel wall, as seen in Fig. 4. Studies done by Adams et al. have shown that the veins and venules in or at a distance from active lesions frequently showed an inflammatory lymphocytic reaction essentially located only in the vessel wall (Adams, 1988; Adams et al., 1985). Fog has also stated that MS lesions typically developed around small veins (Fog, 1964). With the help of longitudinal MICRO data, we could further elucidate whether the abnormal vessel behavior, within or surrounding the lesion, act as a potential source initiating the inflammatory response. However, based on our findings, which show that the MS lesions (even for the smaller size, i.e. ‘small ovoid WMHs’) occur around the normal appearing vessels (with no detectable vessel dilation), we can state that vessel dilation may potentially occur after the inflammation, if these small lesions were occurring in the early stages of the disease. A key question to resolve with a longitudinal study would be: “Are these representative of the development of future lesions?”

Earlier work by Schelling suggested that mechanical effects, such as blood pulsation and enlargement of the perivenous spaces, may lead to dilation of cerebral veins and could cause the immunological phenomena as observed in MS (Schelling, 1986). Allen also noticed wide vascular beds around veins and central widening of the venous tree; these changes testify to an intermittent increase in cerebral pressure (Allen, 1981). Similarly, excessive hypertension could stretch the vessel walls separating the tight junctions between endothelial cells, allowing colloids and other materials to pass through the exposed porous basement membranes (Talbert, 2008).

It has since been proposed that dysfunction of the vessel endothelial cells leads to alterations of the blood vessel architecture. These changes could lead to both enlargement and narrowing of the vessel lumen, along with vessel stiffening (Wardlaw et al., 2013). MS progression and

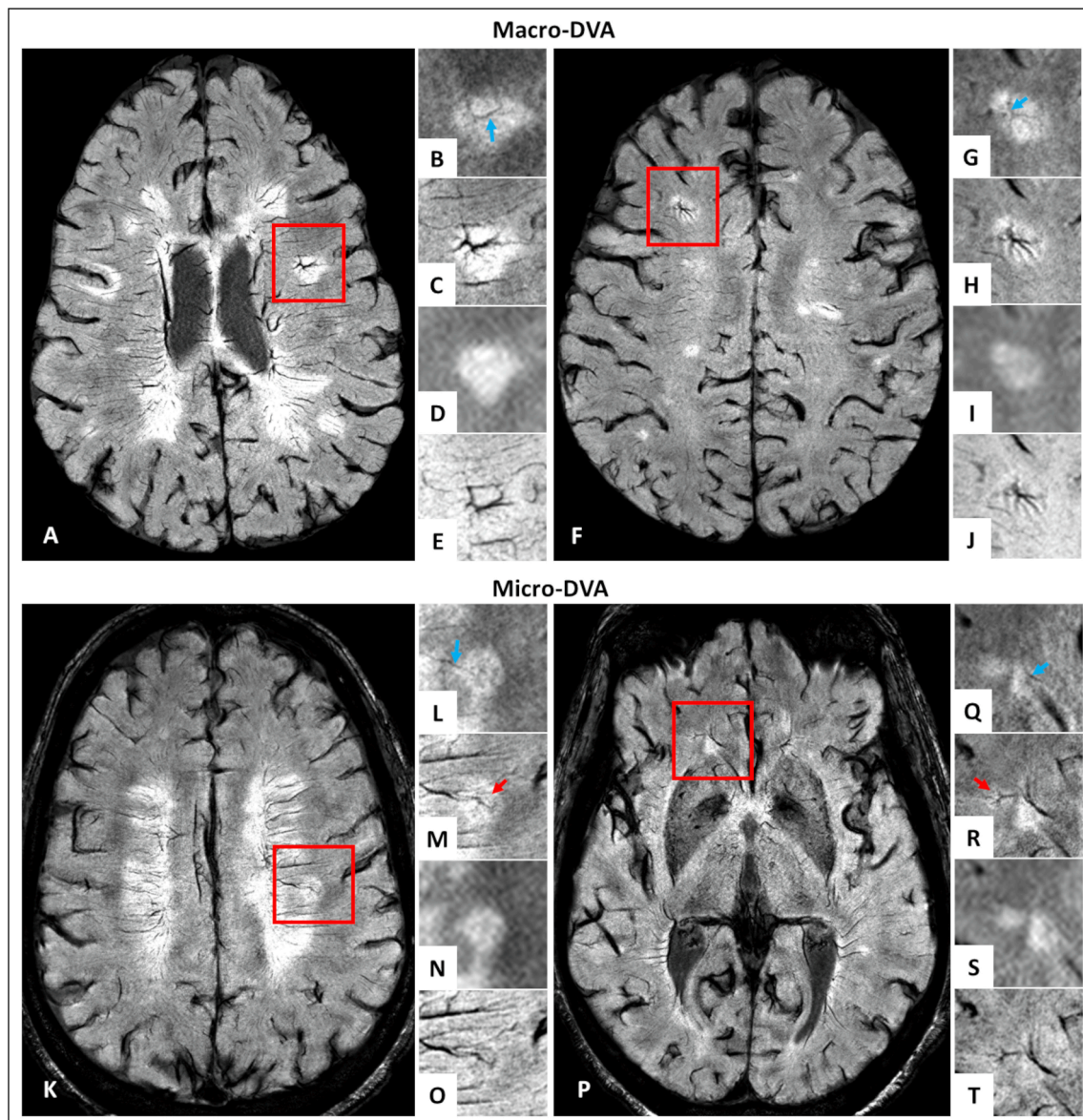


Fig. 7. Post-contrast SWI-FLAIR helps in visualizing vascular angiomas (or macro-DVAs) (A-J) and micro-DVAs (K-T) in MS subjects. Red boxes identify the location of the angiomas on the post-contrast SWI-FLAIR (A, F, K and P), which are shown along with the zoomed insets of pre-contrast SWI-FLAIR (B, G, L and Q), post-contrast SWI-FLAIR (C, H, M and R), FLAIR (D, I, N and S) and SWI data (E, J, O and T). The macro-DVAs show lesion-centric box-like (A-E) or centripetal vascular arrangements (F-J). Similarly, the micro-DVAs indicate a lesion-centric pattern of multiple small vessels, suggesting a developing nature of the DVAs (red arrows). All the four examples were confirmed as venous abnormalities using the pre-contrast data (blue arrows). On the pre-contrast SWI-FLAIR data, the macro-DVAs were almost completely visible, whereas only the primary draining vein were visible for the micro-DVAs (red arrows). (For interpretation of the references to colour in this figure legend, the reader is referred to the web version of this article.)

demyelinated lesions have been correlated with the increased cerebral blood volume (CBV), vasodilation and increased angiogenesis (Papadaki et al., 2012), which could be caused by the increased endothelial cell proliferation and vascular endothelial growth factor (VEGF) and VEGF receptor-1 found to be higher in the MS population compared to normal controls (Girolamo et al., 2014; Holley et al., 2010; Roscoe et al., 2009). Finally, it has been shown that in stroke and restricted retrograde venous hypertension, deep medullary veins could dilate or appear dilated in SWI due to the increased levels of deoxyhemoglobin when there is locally reduced blood flow (Li et al., 2013). Hence, the apparent vessel dilation (Fig. 5) we observed in this study may have been caused by enlargement of perivascular spaces due to mechanical effects, endothelial dysfunction or increased deoxyhemoglobin levels. In MS subjects, there is also evidence of increased blood volume (Haacke et al., 2013) and cerebral blood flow (Bester et al., 2015; Peruzzo et al., 2013) and

reduced mean transit time, the latter being associated with higher disease severity and with the presence of disease one year later in newly diagnosed MS patients (Sowa et al., 2015). Therefore, it is likely that they exhibited a high vascular component within the lesions at this early stage. This could explain the higher PVD within the lesions as compared to the NAWM PVD (Fig. 11).

Another interesting finding was that the small vessels forming the irregular DVAs actually define the shape of the lesion in FLAIR (Fig. 7). These DVAs, which can be classified as atypical DVAs due to their lesion-centric location (Kroll et al., 2010), are comprised of a mesh of veins that appears to have a central nidus and often looks like the Medusa's head (referred to as Caput Medusa) (Lee et al., 1996; Saba, 1998). A number of papers have found signal intensity abnormalities in the tissue surrounding MS lesions (Linscott et al., 2014; Rogers et al., 2018; Sahin et al., 2015; Santucci et al., 2008; Schaller and Graf, 2004; Umino et al.,

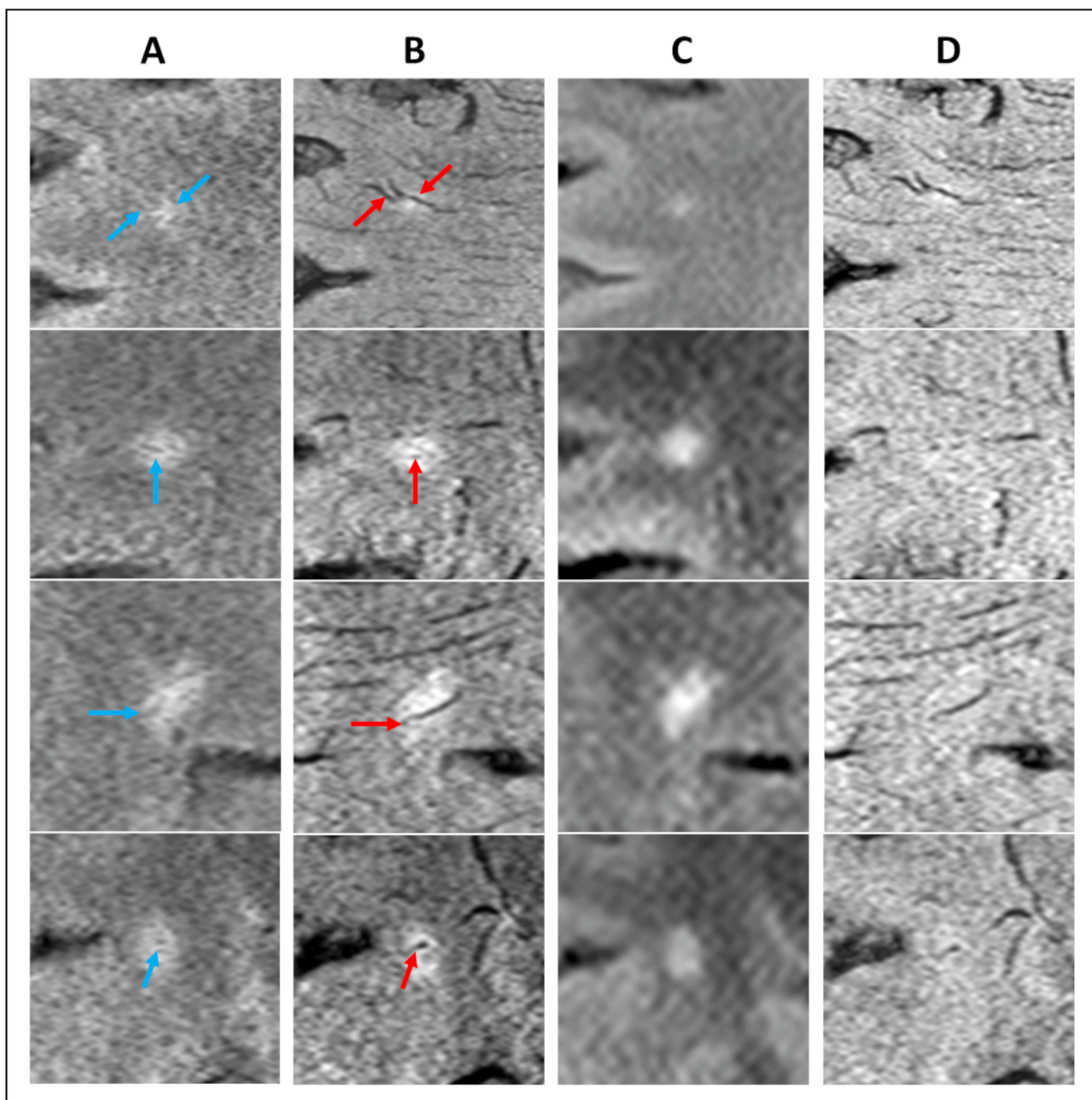


Fig. 8. Four examples of WMHs on healthy controls. The pre-contrast SWI-FLAIR data (A) and post-contrast SWI-FLAIR data (B) display the vasculature associated with the WMHs. The post-contrast SWI-FLAIR offers a better vessel detection (red arrows) than the FLAIR-only data (C) or SWI-only data (D), whereas the subtle enhancement of the vessels on pre-contrast SWI-FLAIR data (blue arrows) confirms that these vessels can be classified as veins. These non-MS WMHs also exhibit a central vein sign similar to the MS lesions. (For interpretation of the references to colour in this figure legend, the reader is referred to the web version of this article.)

2014). Okudera proposed they arose from aplasia, hypoplasia, or occlusion of some part of the medullary venous system (they note it could be from chronic venous hypertension caused by anomalous venous drainage) (Okudera et al., 1999). The presence of the bright signals may be from edema, demyelination or gliosis related to abnormal venous flow (Umino et al., 2014).

Medullary veins of the brain play a key role in draining the blood from white matter. A number of diseases are associated with the medullary veins including hemorrhagic disorders, inflammatory changes that spread along the veins, and neoplasms within the veins (Taoka et al., 2017). The first two may be related to metabolic changes associated with venous wall damage and are implicated in MS. The sub-voxel vessels feeding the medullary veins and eventually the larger ependymal veins pervade the WM and a breakdown of the venous drainage could signal

drastic consequences, including the formation of anastomotic connections (as seen through the development of the DVAs or the formation of perpendicular vessels as shown in Fig. 6). Although the acute signs appear to be an increase in CBV, more chronic lesions and even NAWM appear to have reduced CBV as shown with perfusion weighted imaging methods (Francis et al., 2013; Holland et al., 2012; Peruzzo et al., 2013; Sowa et al., 2015; Steen et al., 2013). Several papers show reduced cerebral blood flow and increased mean transit time in MS lesions at all stages of the disease (Adhya et al., 2006; Sowa et al., 2015). Reduced blood volume was found to correlate with working and secondary verbal memory for clinically isolated syndrome patients (Papadaki et al., 2014). Eventually, veins may atrophy or become constricted due to collagenosis and the effective blood volume would then be expected to decrease in chronic lesions (Haacke et al., 2013). The lesions with low vascularity

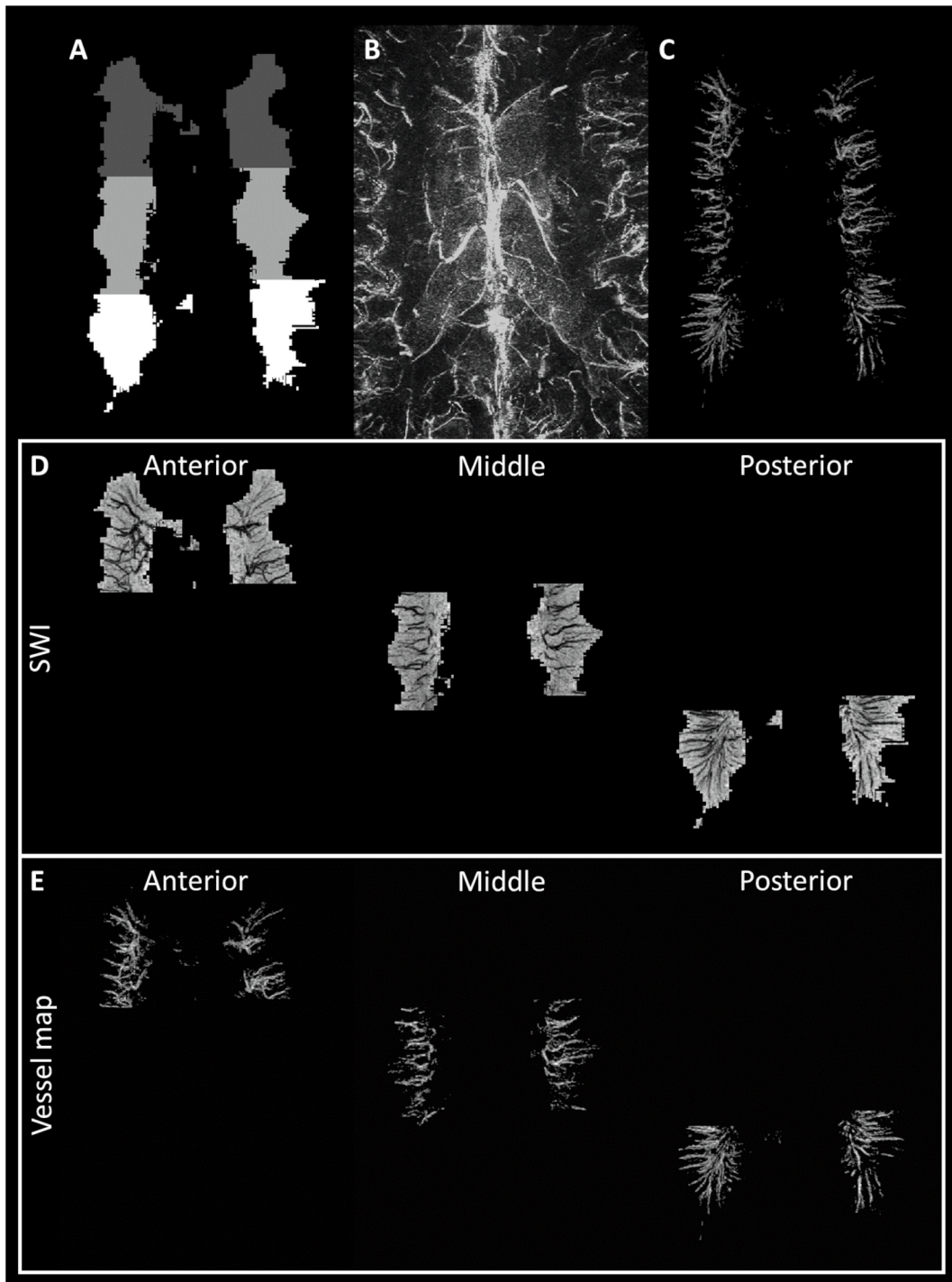


Fig. 9. Mapping the periventricular vasculature. A) The periventricular mask was divided into three equal sections and B) the pre-contrast QSM data was used to discard the major veins. C) The final vessel maps display high contrast for the vascular signal, which allowed the segmentation of the periventricular small vessels, as seen on the SWI data (D), using the proposed vessel tracking approach (E).

may undergo cell death, reduced blood flow and, hence, subsequent vascular atrophy. This may account for the discrepancy between the total number of lesions detected on the FLAIR data and the number of lesions with vascular signs detected on the SWI-FLAIR data in Fig. 3.

There are a few limitations to this study. First, we report on a small number of subjects with two different doses (3 mg/kg and 4 mg/kg). Nevertheless, the main goal of this paper was to demonstrate the efficacy of Ferumoxytol and high-resolution MICRO imaging to reveal the vascularity within the MS lesions; to be able to identify and classify the various vascular anomalies; and to introduce a new method to estimate

the PVD using the MICRO data. For these purposes, the number of cases we have shown here clearly demonstrate these points. As mentioned earlier, the Ferumoxytol dosage was altered from 3 mg/kg to 4 mg/kg for the last three patients, which could affect the visibility of the vasculature and PVD measures, as seen in Fig. 11 where the first three MS patients show a lower NAWM and lesional vessel density. However, the affected visibility of the vessels would be consistent for both the NAWM and lesions PVDs, making the comparison fair between them; similarly demonstrating a higher probability of vessels within the lesions as compared to the periventricular NAWM. On the other hand, the

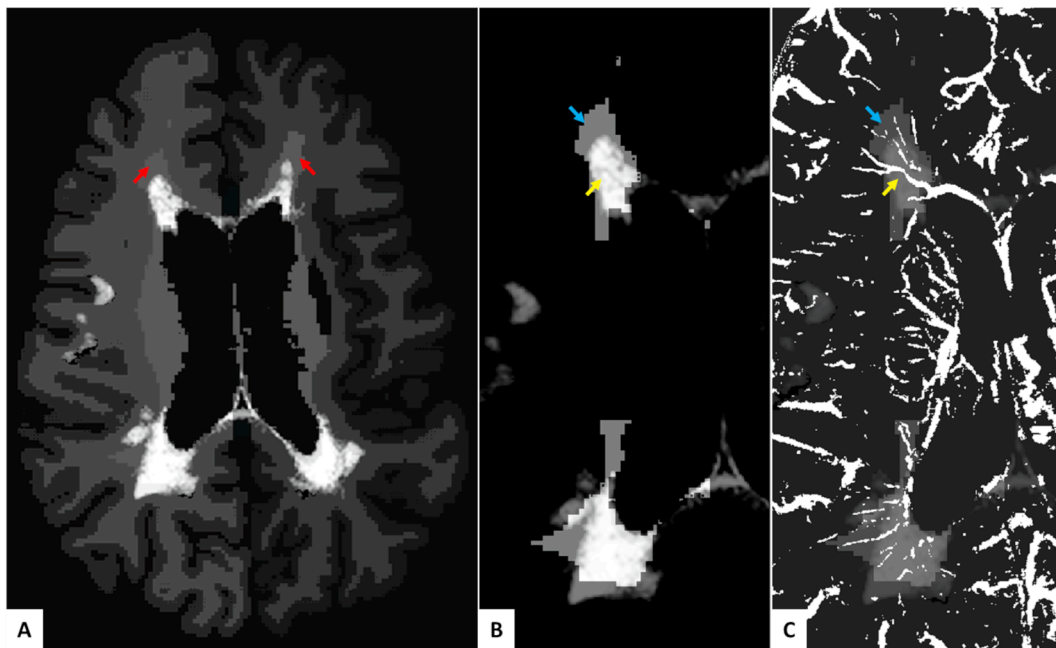


Fig. 10. Lesional and NAWM masks to obtain the PVD. (A) The WM parcellations were used to obtain the periventricular WM (PWM) masks (red arrows), (B) the regions that include lesions within the PWM were used for obtaining lesional PVD (yellow arrows), whereas the regions outside the lesions and within the PWM were used for obtaining the NAWM PVD (blue arrows). The lesion map and PWM are used as overlays for the vessel segmentation results (C). (For interpretation of the references to colour in this figure legend, the reader is referred to the web version of this article.)

differences in TR (30 ms vs 27 ms) and FA (12° vs 15°) between the first three and the last three patients will lead to only very slight changes in the signal behaviour, which will not affect the vascular signal detection on the post-USPIO SWI data. Second, we do not have longitudinal data to monitor these vascular anomalies. The changes in the vasculature over time could well reveal more about the etiology of MS. A future goal of this work is to study lesions of patients with progressive, non-relapsing MS in order to better understand pathophysiology for each MS sub-type.

The proposed MICRO SWI protocol uses a total scan time of 22 mins (that includes two SWI acquisitions for before and after Ferumoxytol administration) and with the amount of information obtained using our protocol, in terms of high resolution MRA (from pre-contrast magnitude data), MRV (from pre-contrast SWI data), cerebral microvasculature map (from post-contrast SWI) and local vascular density along with an addition of a FLAIR acquisition (another 6 mins) for WMH detection; it could potentially make our protocol a powerful clinical tool. This 28 min-protocol can be applied to numerous neuropathological studies that focus on examining the vascular abnormalities in diseased brains. Furthermore, the proposed dual-echo SWI datasets also allow us to obtain quantitative metrics such as QSM and R_2^* maps that are essential for measuring iron content in basal ganglia structures, quantifying local venous oxygenation, etc. In the future, we expect that acquisition times will be reduced using faster sequences, higher compressed sense factors and SEPI. With an injection time of 15 min and scan times perhaps reduced to 7 min each (quite viable in the near future) this could become a practical clinical imaging protocol.

Another consideration is the choice of relatively lower TE (15 ms) for our work than the conventional higher TEs of 20 to 30 ms for SWI processing at 3 T. It is well-known that a dataset acquired with a higher TE would be able to reveal more vasculature. However, the field effects from the sinuses (due to the high susceptibility difference at the air and tissue interfaces) almost destroy the region by the midbrain and mastoid sinuses at that long TE, causing major signal losses in these regions (Buch et al., 2014). Image quality by the sinuses is maintained while the vessels themselves are highlighted by increased susceptibility using the echo time of 15 ms. Conventionally, it is helpful to acquire the SWI data with higher TEs to take advantage of the linear relationship between the

phase behaviour and the TE. However, consider now the fact that the veins will increase in susceptibility from 0.45 ppm to 2.2 ppm in the presence of 4 mg/kg of Ferumoxytol (Liu et al., 2018). To get the same effect in conventional imaging would require a TE of $2.2/0.45 = 4.89$ times higher than usually used. As shown in Fig. 1, the post-contrast SWI (TE = 15 ms) shows a dramatic improvement in vessel contrast as compared to the pre-contrast SWI with a conventionally used TE of 22.5 ms. This data with a TE = 22.5 ms pre-contrast, one would need 72 ms to obtain the same contrast to be equivalent to our TE = 15 ms post-Ferumoxytol data and would then require a TR of 80 ms roughly, which is 3 times longer than the normal scan time. Additionally, there would be almost no signal left in a major part of the brain. So, the key advantage of imaging with Ferumoxytol is to enhance the vasculature and maintain image quality at the same time. We turn this to further advantage by reducing the TE to 15 ms, where the signal loss surrounding the air/tissue interface is now dramatically reduced and image quality remains in tact.

Finally, there is a much higher probability of a vein being present inside the MS lesions as opposed to an artery due to the fact that the arterial blood in the WM, where most of the MS plaques are distributed (Brownell and Hughes, 1962; McDonald et al., 2001; Vellinga et al., 2009), are supplied through arterial branches arising from the cerebral arteries, which are already roughly only 100 μm in size. Therefore, they can be very difficult to visualize, especially once they branch into much smaller arterioles and capillaries (Nonaka et al., 2003). On the other hand, the subcortical WM veins, such as the medullary veins, subependymal veins and their primary confluence veins are located in the periventricular region, where the lesion occurrence is the highest (Charil et al., 2003; Vellinga et al., 2009). These veins are much larger, at approximately 300 μm in size, than the arterial network in the same region (Nonaka et al., 2003). With MICRO imaging, we will not only induce an enhancement of arteries but also further enhance the venous branches. Furthermore, it is well known that the ratio of venous to arterial blood volume is approximately 4:1 (An and Lin, 2002a; 2002b; Hua et al., 2019; McCormick et al., 1991; Mchedlishvili, 1986; Pollard et al., 1996; van Zijl et al., 1998), leaving little signal to arise from the arteries.

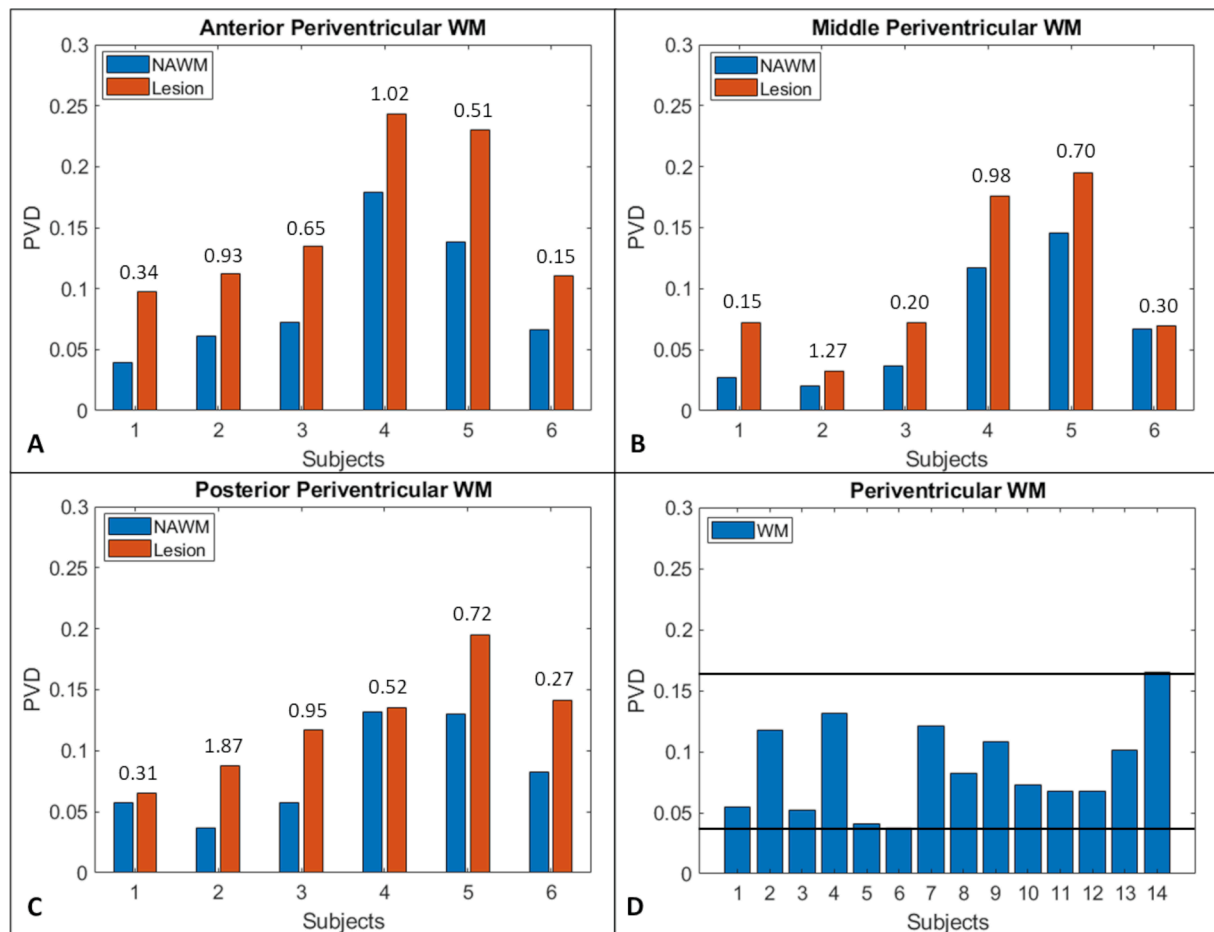


Fig. 11. PVD was estimated from three sub-divisions of the periventricular white matter: (A) anterior, (B) middle and (C) posterior from both NAWM (blue) and lesional white matter (orange), for each MS patient. Similarly, PVD was estimated from the healthy controls (D). The values above the graphs in (A-C) represent the lesion-to-NAWM volume ratio. The NAWM PVD values from the patients lie within the range of WM PVD values estimated in healthy controls (black lines in (D)). However, the difference in PVD for NAWM and lesions was found to be significant ($p < 0.05$). (For interpretation of the references to colour in this figure legend, the reader is referred to the web version of this article.)

Nevertheless, the specificity of vessel classification into major arteries and veins is reduced due to the presence of Ferumoxytol in blood. Hence, the vascular anomalies, as categorized in this paper, could potentially be composed of both arteries and veins. However, as highlighted using the blue arrows in the Figs. 5, 6 and 7, the pre-contrast SWI data were able to confirm that these vascular anomalies (except for the small ovoid category, where the vessels were too small to be detected on the pre-contrast SWI) were part of the venous network. There is still a possibility of a relatively small contribution of the arterial network (~20%) being present in MS lesions and the inability to separate the veins and arteries is one of the major limitations, particularly for vessels on the order of or smaller than 100 μm . In order to address this, the total vascular density was also calculated in this work to compare the lesions and *peri*-lesional vessel density, which can include both arteries and veins. A future direction will be to develop the technology to separate small arteries from small veins of the microvasculature from the SWI data acquired at multiple timepoints with increasing Ferumoxytol concentration levels. This separation of small arteries and veins will be essential for cerebral small vessel disease, for example, which is a highly prevalent disease that is known to affect the small vessels of the brain including the arterioles, venules and capillaries (Pantoni, 2010); and causes vascular WM abnormalities that can mimic MS lesions.

In conclusion, by inducing an additional susceptibility into the blood using Ferumoxytol, the vascular abnormalities in the RRMS patients were revealed. Small vessel density measures, obtained by combining the proposed vessel mapping and tracking approach with a lesion

detection method, showed higher intra-lesional vascular density as compared to the NAWM in the periventricular region. MICRO imaging has the potential to monitor the venous vasculature present in MS lesions, catalogue their characteristics and compare the vascular structures spatially to the presence of MS lesions which may provide new insight into the pathophysiology of MS.

Funding sources

This work was supported in part by the sub-organizations of National Institutes of Health (NIH): National Institute on Aging (grant number: R56-AG060822), National Institute of Neurological Disorders and Stroke (grant number: R01-NS108491), Eunice Kennedy Shriver National Institute of Child Health and Human Development (grant number: R21-HD094424) and National Heart, Lung, And Blood Institute (grant number: R44-HL145826). The content is solely the responsibility of the authors and does not necessarily represent the official views of the National Institutes of Health. This work was also supported by the Silverman Brain Injury Research Fund at Wayne State University.

CRediT authorship contribution statement

Sagar Buch: Conceptualization, Methodology, Investigation, Software, Formal analysis, Writing - original draft. **Karthikeyan Subramanian:** Methodology, Investigation, Formal analysis, Writing - review & editing. **Pavan K. Jella:** Data curation, Methodology,

Investigation. **Yongsheng Chen:** Methodology. **Zhen Wu:** Writing - review & editing, Formal analysis. **Kamran Shah:** Writing - review & editing. **Evanthia Bernitsas:** Methodology, Data curation. **Yulin Ge:** Funding acquisition, Supervision, Writing - review & editing. **E. Mark Haacke:** Conceptualization, Methodology, Supervision, Funding acquisition, Writing - review & editing.

Declaration of Competing Interest

The authors declare that they have no known competing financial interests or personal relationships that could have appeared to influence the work reported in this paper.

Acknowledgements

The authors would like to thank our MRI technicians, Zahid Latif and Yang Xuan, for their efforts in collecting and organizing the data. The authors would also like to thank the participants that volunteered for this study. The views, opinions, and/or findings contained in this report are those of the author(s) and should not be construed as an official government position, policy or decision unless so designated by other documentation.

References

- Abdul-Rahman, H.S., Gdeisat, M.A., Burton, D.R., Lalor, M.J., Lilley, F., Moore, C.J., 2007. Fast and robust three-dimensional best path phase unwrapping algorithm. *Appl. Opt.* 46, 6623–6635. <https://doi.org/10.1364/AO.46.006623>.
- Adams, C.W., 1975. The onset and progression of the lesion in multiple sclerosis. *J. Neurol. Sci.* 25, 165–182. [https://doi.org/10.1016/0022-510x\(75\)90138-0](https://doi.org/10.1016/0022-510x(75)90138-0).
- Adams, C.W.M., 1988. Perivascular iron deposition and other vascular damage in multiple sclerosis. *J. Neurol. Neurosurg. Psychiatry* 51, 260–265. <https://doi.org/10.1136/jnnp.51.2.260>.
- Adams, C.W.M., Poston, R.N., Buk, S.J., Sidhu, Y.S., Vipond, H., 1985. Inflammatory vasculitis in multiple sclerosis. *J. Neurol. Sci.* [https://doi.org/10.1016/0022-510x\(85\)90139-x](https://doi.org/10.1016/0022-510x(85)90139-x).
- Adhya, S., Johnson, G., Herbert, J., Jaggi, H., Babb, J.S., Grossman, R.I., Ingles, M., 2006. Pattern of hemodynamic impairment in multiple sclerosis: Dynamic susceptibility contrast perfusion MR imaging at 3.0 T. *NeuroImage*. <https://doi.org/10.1016/j.neuroimage.2006.08.008>.
- Allen, I.V., 1981. The pathology of multiple sclerosis - fact, fiction and hypothesis. *Neuropathol. Appl. Neurobiol.* 7, 169–182. <https://doi.org/10.1111/j.1365-2990.1981.tb00087.x>.
- An, H., Lin, W., 2002a. Cerebral venous and arterial blood volumes can be estimated separately in humans using magnetic resonance imaging. *Magn. Reson. Med.* 48, 583–588. <https://doi.org/10.1002/mrm.10257>.
- An, H., Lin, W., 2002b. Cerebral oxygen extraction fraction and cerebral venous blood volume measurements using MRI: effects of magnetic field variation. *Magn. Reson. Med.* 47, 958–966. <https://doi.org/10.1002/mrm.10148>.
- Ashburner, J., Friston, K., 1997. Multimodal image coregistration and partitioning—a unified framework. *NeuroImage* 6, 209–217. <https://doi.org/10.1006/nimg.1997.0290>.
- Barnett, M.H., Prineas, J.W., 2004. Relapsing and remitting multiple sclerosis: pathology of the newly forming lesion. *Ann. Neurol.* 55, 458–468. <https://doi.org/10.1002/ana.20016>.
- Bartko, J.J., 1991. Measurement and reliability: statistical thinking considerations. *Schizophr. Bull.* 17, 483–489. <https://doi.org/10.1093/schbul/17.3.483>.
- Bester, M., Forkert, N.D., Stellmann, J.P., Aly, L., Drabik, A., Young, K.L., Heesen, C., Fiehler, J., Siemonsen, S., 2015. Increased perfusion in normal appearing white matter in high inflammatory multiple sclerosis patients. *PLoS ONE*. <https://doi.org/10.1371/journal.pone.0119356>.
- Bourneville, D.M., Guérard, L., 1869. *De la sclérose en plaques disséminées*. Delahaye.
- Brownell, B., Hughes, J.T., 1962. The distribution of plaques in the cerebrum in multiple sclerosis. *J. Neurol. Neurosurg. Psychiatry* 25, 315–320. <https://doi.org/10.1136/jnnp.25.4.315>.
- Buch, S., Liu, S., Ye, Y., Cheng, Y.-C.N., Neelavalli, J., Haacke, E.M., 2014. Susceptibility mapping of air, bone, and calcium in the head. *Magn. Reson. Med.* [n/a/n/a. https://doi.org/10.1002/mrm.25350](https://doi.org/10.1002/mrm.25350).
- Buch, S., Wang, Y., Park, M.-G., Jella, P.K., Hu, J., Chen, Y., Shah, K., Ge, Y., Haacke, E. M., 2020. Subvoxel vascular imaging of the midbrain using USPIO-Enhanced MRI. *NeuroImage* 220. <https://doi.org/10.1016/j.neuroimage.2020.117106>.
- Caprio, M., Russo, C., Giugliano, A., Ragucci, M., Mancini, M., 2016. Vascular Disease in Patients with Multiple Sclerosis: A Review. *J. Vasc. Med. Surg.* 4, 1–12. <https://doi.org/10.4172/2329-6925.1000259>.
- Charcot, J.M., 1868. *Histologie de la sclérose en plaques*. Gaz. Hôpitaux.
- Charil, A., Zijdenbos, A.P., Taylor, J., Boelman, C., Worsley, K.J., Evans, A.C., Dagher, A., 2003. Statistical mapping analysis of lesion location and neurological disability in multiple sclerosis: application to 452 patient data sets. *NeuroImage* 19, 532–544. [https://doi.org/10.1016/s1053-8119\(03\)00117-4](https://doi.org/10.1016/s1053-8119(03)00117-4).
- Chavhan, G.B., Babyn, P.S., Thomas, B., Shroff, M.M., Haacke, E.M., 2009. Principles, techniques, and applications of T2*-based MR imaging and its special applications. *Radiogr. Rev. Publ. Radiol. Soc. N. Am. Inc* 29, 1433–1449. <https://doi.org/10.1148/rg.295095034>.
- Chen, Y., Liu, S., Buch, S., Hu, J., Kang, Y., Haacke, E.M., 2018. An interleaved sequence for simultaneous magnetic resonance angiography (MRA), susceptibility weighted imaging (SWI) and quantitative susceptibility mapping (QSM). *Magn. Reson. Imaging* 47, 1–6. <https://doi.org/10.1016/j.mri.2017.11.005>.
- Cheng, A.-L., Batool, S., McCreary, C.R., Lauzon, M.L., Frayne, R., Goyal, M., Smith, E.E., 2013. Susceptibility-Weighted Imaging is More Reliable Than T2*-Weighted Gradient-Recalled Echo MRI for Detecting Microbleeds. *Stroke* 44, 2782–2786. <https://doi.org/10.1161/STROKEAHA.113.002267>.
- Cicchetti, D.V., 1994. Guidelines, criteria and rules of thumbs for evaluating normed and standardized assessment instruments in psychology. *Psychol. Assess.* 284–290.
- Collignon, A., Maes, F., Delaere, D., Vandermeulen, D., Suetens, P., Marchal, G., 1995. Automated multi-modality image registration based on information theory. *Bizais*.
- Collins, D.L., Neelin, P., Peters, T.M., Evans, A.C., 1994. Automatic 3D intersubject registration of MR volumetric data in standardized Talairach space. *J. Comput. Assist. Tomogr.* 18, 192–205.
- Dendrou, C.A., Fugger, L., Friese, M.A., 2015. Immunopathology of multiple sclerosis. *Nat. Rev. Immunol.* 15, 545–558. <https://doi.org/10.1038/nri3871>.
- Descoteaux, M., Collins, D.L., Siddiqi, K., 2008. A geometric flow for segmenting vasculature in proton-density weighted MRI. *Med. Image Anal.* 12, 497–513. <https://doi.org/10.1016/j.media.2008.02.003>.
- Fischl, B., Salat, D.H., Busa, E., Albert, M., Dieterich, M., Haselgrove, C., van der Kouwe, A., Killiany, R., Kennedy, D., Klaveness, S., Montillo, A., Makris, N., Rosen, B., Dale, A.M., 2002. Whole brain segmentation: automated labeling of neuroanatomical structures in the human brain. *Neuron* 33, 341–355. [https://doi.org/10.1016/s0896-6273\(02\)00569-x](https://doi.org/10.1016/s0896-6273(02)00569-x).
- Fischl, B., van der Kouwe, A., Destrieux, C., Halgren, E., Ségonne, F., Salat, D.H., Busa, E., Seidman, L.J., Goldstein, J., Kennedy, D., Caviness, V., Makris, N., Rosen, B., Dale, A. M., 2004. Automatically parcellating the human cerebral cortex. *Cereb. Cortex N. Y. N* 1991 (14), 11–22. <https://doi.org/10.1093/cercor/bhg087>.
- Fog, T., 1964. ON THE VESSEL-PLAQUE RELATIONSHIPS IN THE BRAIN IN MULTIPLE SCLEROSIS. *Acta Neurol. Scand.* <https://doi.org/10.1111/j.1600-0404.1964.tb04716.x>.
- Francis, P.L., Jakubovic, R., O'Connor, P., Zhang, L., Eilaghi, A., Lee, L., Carroll, T.J., Mouannes-Srouf, J., Feinstein, A., Aviv, R.I., 2013. Robust perfusion deficits in cognitively impaired patients with secondary-progressive Multiple Sclerosis. *Am. J. Neuroradiol.* <https://doi.org/10.3174/ajnr.A3148>.
- Frangi, A., Niessen, W., Vincken, K., Viergever, M., 1998. Multiscale vessel enhancement filtering, in: *Medical Image Computing and Computer Assisted Intervention - MICCAI'98*, pp. 130–137.
- Gaitán, M.I., De Alwis, M.P., Sati, P., Nair, G., Reich, D.S., 2013. Multiple sclerosis shrinks intralobular, and enlarges extralobular, brain parenchymal veins. *Neurology* 80, 145–151. <https://doi.org/10.1212/WNL.0b013e31827b916f>.
- Ge, Y., Zhang, Z., Lu, H., Tang, L., Jaggi, H., Herbert, J., Babb, J.S., Rusinek, H., Grossman, R.I., 2012. Characterizing brain oxygen metabolism in patients with multiple sclerosis with T2-relaxation-under-spin-tagging MRI. *J. Cereb. Blood Flow Metab.* 32, 403–412. <https://doi.org/10.1038/jcbfm.2011.191>.
- Ge, Y., Zohrabian, V.M., Osa, E.-O., Xu, J., Jaggi, H., Herbert, J., Haacke, E.M., Grossman, R.I., 2009. Diminished visibility of cerebral venous vasculature in multiple sclerosis by susceptibility-weighted imaging at 3.0 Tesla. *J. Magn. Reson. Imaging* 29, 1190–1194. <https://doi.org/10.1002/jmri.21758>.
- Girolamo, F., Coppola, C., Ribatti, D., Trojano, M., 2014. Angiogenesis in multiple sclerosis and experimental autoimmune encephalomyelitis. *Acta Neuropathol. Commun.* 2, 84. <https://doi.org/10.1186/s40478-014-0084-z>.
- Grabner, G., Dal-Bianco, A., Schernthaner, M., Vass, K., Lassmann, H., Trattnig, S., 2011. Analysis of multiple sclerosis lesions using a fusion of 3.0 T FLAIR and 7.0 T SWI phase: FLAIR SWI. *J. Magn. Reson. Imaging JMRI* 33, 543–549. <https://doi.org/10.1002/jmri.22452>.
- Haacke, E.M., Chen, Y., Utraiainen, D., Wu, B., Wang, Y., Xia, S., He, N., Zhang, C., Wang, X., Lagana, M.M., Luo, Y., Fatemi, A., Liu, S., Gharabaghi, S., Wu, D., Sethi, S. K., Huang, F., Sun, T., Qu, F., Yadav, B.K., Ma, X., Bai, Y., Wang, M., Cheng, J., Yan, F., 2020. SStrategically Acquired Gradient Echo (STAGE) imaging, part III: Technical advances and clinical applications of a rapid multi-contrast multi-parametric brain imaging method. *Magn. Reson. Imaging* 65, 15–26. <https://doi.org/10.1016/j.mri.2019.09.006>.
- Haacke, E.M., DelProposto, Z.S., Chaturvedi, S., Sehgal, V., Tenzer, M., Neelavalli, J., Kido, D., 2007. Imaging cerebral amyloid angiopathy with susceptibility-weighted imaging. *AJNR Am. J. Neuroradiol.* 28, 316–317.
- Haacke, E.M., Li, M., Juvvugunta, F., 2013. Tissue similarity maps (TSMs): A new means of mapping vascular behavior and calculating relative blood volume in perfusion weighted imaging. *Magn. Reson. Imaging*. <https://doi.org/10.1016/j.mri.2012.10.005>.
- Haacke, E.M., Xu, Y., Cheng, Y.-C.N., Reichenbach, J.R., 2004. Susceptibility weighted imaging (SWI). *Magn. Reson. Med.* 52, 612–618. <https://doi.org/10.1002/mrm.20198>.
- Holland, C.M., Charil, A., Csapo, I., Liptak, Z., Ichise, M., Khoury, S.J., Bakshi, R., Weiner, H.L., Guttmann, C.R.G., 2012. The Relationship between Normal Cerebral Perfusion Patterns and White Matter Lesion Distribution in 1,249 Patients with Multiple Sclerosis. *J. Neuroimaging*. <https://doi.org/10.1111/j.1552-6569.2011.00585.x>.

- Holley, J.E., Newcombe, J., Whatmore, J.L., Gutowski, N.J., 2010. Increased blood vessel density and endothelial cell proliferation in multiple sclerosis cerebral white matter. *Neurosci. Lett.* 470, 65–70. <https://doi.org/10.1016/j.neulet.2009.12.059>.
- Hua, J., Liu, P., Kim, T., Donahue, M., Rane, S., Chen, J.J., Qin, Q., Kim, S.-G., 2019. MRI techniques to measure arterial and venous cerebral blood volume. *NeuroImage* 187, 17–31. <https://doi.org/10.1016/j.neuroimage.2018.02.027>.
- Kroll, H., Soares, B.P., Saloner, D., Dillon, W.P., Wintermark, M., 2010. Perfusion-CT of Developmental Venous Anomalies: Typical and Atypical Hemodynamic Patterns. *J. Neuroradiol. J. Neuroradiol.* 37, 239–242. <https://doi.org/10.1016/j.neurad.2009.09.002>.
- Lee, B.C., Vo, K.D., Kido, D.K., Mukherjee, P., Reichenbach, J., Lin, W., Yoon, M.S., Haacke, M., 1999. MR high-resolution blood oxygenation level-dependent venography of occipital (low-flow) vascular lesions. *AJNR Am. J. Neuroradiol.* 20, 1239–1242.
- Lee, C., Pennington, M.A., Kenney, C.M., 1996. MR evaluation of developmental venous anomalies: medullary venous anomaly of venous angiomata. *AJNR Am. J. Neuroradiol.* 17, 61–70.
- Li, M., Hu, J., Miao, Y., Shen, H., Tao, D., Yang, Z., Li, Q., Xuan, S.Y., Raza, W., Alzubaidi, S., Haacke, E.M., 2013. In vivo measurement of oxygenation changes after stroke using susceptibility weighted imaging filtered phase data. *PLoS One* 8. <https://doi.org/10.1371/journal.pone.0063013>.
- Linscott, L.L., Leach, J.L., Zhang, B., Jones, B.V., 2014. Brain parenchymal signal abnormalities associated with developmental venous anomalies in children and young adults. *Am. J. Neuroradiol.* <https://doi.org/10.3174/ajnr.A3960>.
- Liu, S., Brisset, J.C., Hu, J., Haacke, E.M., Ge, Y., 2018. Susceptibility weighted imaging and quantitative susceptibility mapping of the cerebral vasculature using ferromagnetic J. Magn. Reson. Imaging. <https://doi.org/10.1002/jmri.25809>.
- Maggi, P., Mazzoni, L.N., Moretti, M., Grammatico, M., Chiti, S., Massacesi, L., 2015. SWI enhances vein detection using gadolinium in multiple sclerosis. *Acta Radiol. Open.* <https://doi.org/10.1177/2047981614560938>.
- McCormick, P.W., Stewart, M., Goetting, M.G., Balakrishnan, G., 1991. Regional cerebrovascular oxygen saturation measured by optical spectroscopy in humans. *Stroke* 22, 596–602. <https://doi.org/10.1161/01.str.22.5.596>.
- McDonald, W.I., Compston, A., Edan, G., Goodkin, D., Hartung, H.P., Lublin, F.D., McFarland, H.F., Paty, D.W., Polman, C.H., Reingold, S.C., Sandberg-Wollheim, M., Sibley, W., Thompson, A., van den Noort, S., Weinshenker, B.Y., Wolinsky, J.S., 2001. Recommended diagnostic criteria for multiple sclerosis: guidelines from the International Panel on the diagnosis of multiple sclerosis. *Ann. Neurol.* 50, 121–127. <https://doi.org/10.1002/ana.1032>.
- McGraw, K., Wong, S., 1996. Forming Inferences About Some Intraclass Correlation Coefficients. *Psychol. Methods* 1, 30–46.
- Mchedlishvili, G., 1986. *Arterial behavior and blood circulation in brain*. Plenum Press, New York.
- Mistry, N., Abdel-Fahim, R., Samaraweera, A., Mouglin, O., Tallantyre, E., Tench, C., Jaspán, T., Morris, P., Morgan, P.S., Evangelou, N., 2016. Imaging central veins in brain lesions with 3-T T2*-weighted magnetic resonance imaging differentiates multiple sclerosis from microangiopathic brain lesions. *Mult. Scler. Houndmills Basingstoke Engl.* 22, 1289–1296. <https://doi.org/10.1177/1352458515616700>.
- Mittal, S., Wu, Z., Neelavalli, J., Haacke, E.M., 2009. Susceptibility-weighted imaging: technical aspects and clinical applications, part 2. *AJNR Am. J. Neuroradiol.* 30, 232–252. <https://doi.org/10.3174/ajnr.A1461>.
- Nonaka, H., Akima, M., Hatori, T., Nagayama, T., Zhang, Z., Ihara, F., 2003. Microvasculature of the human cerebral white matter: arteries of the deep white matter. *Neuropathol. Off. J. Jpn. Soc. Neuropathol.* 23, 111–118. <https://doi.org/10.1046/j.1440-1789.2003.00486.x>.
- Okudera, T., Huang, Y.P., Fukusumi, A., Nakamura, Y., Hatazawa, J., Uemura, K., 1999. Micro-angiographical studies of the medullary venous system of the cerebral hemisphere. *Neuropathology.* <https://doi.org/10.1046/j.1440-1789.1999.00215.x>.
- Pantoni, L., 2010. Cerebral small vessel disease: from pathogenesis and clinical characteristics to therapeutic challenges. *Lancet Neurol.* 9, 689–701. [https://doi.org/10.1016/S1474-4422\(10\)70104-6](https://doi.org/10.1016/S1474-4422(10)70104-6).
- Papadaki, E.Z., Mastorodemos, V.C., Amanakis, E.Z., Tsekouras, K.C., Papadakis, A.E., Tsavalas, N.D., Simos, P.G., Karantanas, A.H., Plaitakis, A., Maris, T.G., 2012. White matter and deep gray matter hemodynamic changes in multiple sclerosis patients with clinically isolated syndrome. *Magn. Reson. Med.* 68, 1932–1942. <https://doi.org/10.1002/mrm.24194>.
- Papadaki, E.Z., Simos, P.G., Panou, T., Mastorodemos, V.C., Maris, T.G., Karantanas, A.H., Plaitakis, A., 2014. Hemodynamic evidence linking cognitive deficits in clinically isolated syndrome to regional brain inflammation. *J. Neurol. Eur.* <https://doi.org/10.1111/ene.12338>.
- Peruzzo, D., Castellaro, M., Calabrese, M., Veronese, E., Rinaldi, F., Bernardi, V., Favaretto, A., Gallo, P., Bertoldo, A., 2013. Heterogeneity of cortical lesions in multiple sclerosis: An MRI perfusion study. *J. Cereb. Blood Flow Metab.* <https://doi.org/10.1038/jcbfm.2012.192>.
- Pollard, V., Prough, D.S., DeMelo, A.E., Deyo, D.J., Uchida, T., Stoddart, H.F., 1996. Validation in volunteers of a near-infrared spectroscope for monitoring brain oxygenation in vivo. *Anesth. Analg.* 82, 269–277. <https://doi.org/10.1097/0000539-199602000-00010>.
- Poser, C.M., 1986. Pathogenesis of multiple sclerosis. A critical reappraisal. *Acta Neuropathol. (Berl.)* 71, 1–10. <https://doi.org/10.1007/BF00687954>.
- Reichenbach, J.R., Jonetz-Mentzel, L., Fitzek, C., Haacke, E.M., Kido, D.K., Lee, B.C., Kaiser, W.A., 2001. High-resolution blood oxygen-level dependent MR venography (HRBV): a new technique. *Neuroradiology* 43, 364–369.
- Reichenbach, J.R., Venkatesan, R., Schilling, D.J., Kido, D.K., Haacke, E.M., 1997. Small vessels in the human brain: MR venography with deoxyhemoglobin as an intrinsic contrast agent. *Radiology* 204, 272–277. <https://doi.org/10.1148/radiology.204.1.9205259>.
- Rogers, D.M., Shah, L.M., Wiggins, R.H., 2018. The central vein: FLAIR signal abnormalities associated with developmental venous anomalies in patients with multiple sclerosis. *Am. J. Neuroradiol.* <https://doi.org/10.3174/ajnr.A5819>.
- Roscoe, W.A., Welsh, M.E., Carter, D.E., Karlik, S.J., 2009. VEGF and angiogenesis in acute and chronic MOG(35–55) peptide induced EAE. *J. Neuroimmunol.* 209, 6–15. <https://doi.org/10.1016/j.jneuroim.2009.01.009>.
- Saba, P.R., 1998. The caput medusae sign. *Radiology* 207, 599–600. <https://doi.org/10.1148/radiology.207.3.9609879>.
- Sahin, N., Solak, A., Genc, B., Bilgic, N., 2015. Atypical developmental venous anomaly associated with contrast enhancement and hyperperfusion in the surrounding basal ganglia. *Quant. Imaging Med. Surg.* <https://doi.org/10.3978/j.issn.2223-4292.2014.09.02>.
- Santucci, G.M., Leach, J.L., Ying, J., Leach, S.D., Tomsick, T.A., 2008. Brain parenchymal signal abnormalities associated with developmental venous anomalies: Detailed MR imaging assessment. *Am. J. Neuroradiol.* <https://doi.org/10.3174/ajnr.A1090>.
- Sati, P., George, I.C., Shea, C.D., Gaitán, M.I., Reich, D.S., 2012. FLAIR*: A Combined MR Contrast Technique for Visualizing White Matter Lesions and Parenchymal Veins. *Radiology* 265, 926–932. <https://doi.org/10.1148/radiol.12120208>.
- Sati, P., Oh, J., Constable, R.T., Evangelou, N., Guttman, C.R.G., Henry, R.G., Klawiter, E.C., Mainero, C., Massacesi, L., McFarland, H., Nelson, F., Ontaneda, D., Rauscher, A., Rooney, W.D., Samaraweera, A.P.R., Shinohara, R.T., Sobel, R.A., Solomon, A.J., Treaba, C.A., Wuerfel, J., Zivadinov, R., Sicotte, N.L., Pelletier, D., Reich, D.S., N.A.I.M.S. Cooperative, 2016a. The central vein sign and its clinical evaluation for the diagnosis of multiple sclerosis: a consensus statement from the North American Imaging in Multiple Sclerosis Cooperative. *Nat. Rev. Neurol.* 12, 714–722. <https://doi.org/10.1038/nrneuro.2016.166>.
- Sati, P., Oh, J., Todd Constable, R., Evangelou, N., Guttman, C.R.G., Henry, R.G., Klawiter, E.C., Mainero, C., Massacesi, L., McFarland, H., Nelson, F., Ontaneda, D., Rauscher, A., Rooney, W.D., Samaraweera, A.P.R., Shinohara, R.T., Sobel, R.A., Solomon, A.J., Treaba, C.A., Wuerfel, J., Zivadinov, R., Sicotte, N.L., Pelletier, D., Reich, D.S., 2016b. The central vein sign and its clinical evaluation for the diagnosis of multiple sclerosis: A consensus statement from the North American Imaging in Multiple Sclerosis Cooperative. *Nat. Rev. Neurol.* 12, 714–722. <https://doi.org/10.1038/nrneuro.2016.166>.
- Schaller, B., Graf, R., 2004. Cerebral venous infarction: The pathophysiological concept. *Cerebrovasc. Dis.* 18, 179–188. <https://doi.org/10.1159/000079939>.
- Schelling, F., 1986. *Venous Reflux Into the Skull or Spine: Med. Hypothesis* 21, 141–148.
- Schmidt, P., 2017. Bayesian inference for structured additive regression models for large-scale problems with applications to medical imaging. Ludwig-Maximilians-Universität, München, Munich.
- Schmidt, P., Gaser, C., Arsic, M., Buck, D., Förschler, A., Berthele, A., Hoshi, M., Ilg, R., Schmid, V.J., Zimmer, C., Hemmer, B., Mühlau, M., 2012. An automated tool for detection of FLAIR-hyperintense white-matter lesions in Multiple Sclerosis. *NeuroImage* 59, 3774–3783. <https://doi.org/10.1016/j.neuroimage.2011.11.032>.
- Schweser, F., Deistung, A., Lehr, B.W., Reichenbach, J.R., 2011. Quantitative imaging of intrinsic magnetic tissue properties using MRI signal phase: an approach to in vivo brain iron metabolism? *NeuroImage* 54, 2789–2807. <https://doi.org/10.1016/j.neuroimage.2010.10.070>.
- Shen, Y., Hu, J., Eteer, K., Chen, Y., Buch, S., Alhourani, H., Shah, K., Jiang, Q., Ge, Y., Haacke, E.M., 2020. Detecting sub-voxel microvasculature with USPIO-enhanced susceptibility-weighted MRI at 7 T. *Magn. Reson. Imaging.* <https://doi.org/10.1016/j.jmri.2019.12.010>.
- Shrout, P.E., Fleiss, J.L., 1979. Intraclass correlations: uses in assessing rater reliability. *Psychol. Bull.* 86, 420–428. <https://doi.org/10.1037/0033-2909.86.2.420>.
- Sowa, P., Bjørnerud, A., Nygaard, G.O., Damangir, S., Spulber, G., Celius, E.G., Due-Tønnessen, P., Harbo, H.F., Beyer, M.K., 2015. Reduced perfusion in white matter lesions in multiple sclerosis. *Eur. J. Radiol.* <https://doi.org/10.1016/j.ejrad.2015.09.007>.
- Sparacia, G., Speciale, C., Banco, A., Bencivinni, F., Midiri, M., 2016. Accuracy of SWI sequences compared to T2*-weighted gradient echo sequences in the detection of cerebral cavernous malformations in the familial form. *Neuroradiol. J.* 29, 326–335. <https://doi.org/10.1177/1971400916665376>.
- Steen, C., D'haeseleer, M., Hoogduin, J.M., Fierens, Y., Cambron, M., Mostert, J.P., Dorothea, D.J., Koch, M.W., De Keyser, J., 2013. Cerebral white matter blood flow and energy metabolism in multiple sclerosis. *Mult. Scler. J.* <https://doi.org/10.1177/1352458513477228>.
- Studholme, C., Hill, D.L.G., Hawkes, D.J., 1999. An overlap invariant entropy measure of 3D medical image alignment. *Pattern Recognit.* 32, 71–86. [https://doi.org/10.1016/S0031-3203\(98\)00091-0](https://doi.org/10.1016/S0031-3203(98)00091-0).
- Talbot, D.G., 2008. Raised venous pressure as a factor in multiple sclerosis. *Med. Hypotheses.* <https://doi.org/10.1016/j.mehy.2007.10.009>.
- Tallantyre, E.C., Dixon, J.E., Donaldson, I., Owens, T., Morgan, P.S., Morris, P.G., Evangelou, N., 2011. Ultra-high-field imaging distinguishes MS lesions from asymptomatic white matter lesions. *Neurology* 76, 534–539. <https://doi.org/10.1212/WNL.0b013e31820b7630>.
- Tan, L.L., Van Schijndel, R.A., Pouwels, P.J.W., Van Walderveen, M.A.A., Reichenbach, J.R., Manoliu, R.A., Barkhof, F., 2000. MR venography of multiple sclerosis. *Am. J. Neuroradiol.*
- Tang, J., Liu, S., Neelavalli, J., Cheng, Y.C.N., Buch, S., Haacke, E.M., 2013. Improving susceptibility mapping using a threshold-based K-space/image domain iterative reconstruction approach. *Magn. Reson. Med.* 69, 1396–1407. <https://doi.org/10.1002/mrm.24384>.

- Taoka, T., Fukusumi, A., Miyasaka, T., Kawai, H., Nakane, T., Kichikawa, K., Naganawa, S., 2017. Structure of the medullary veins of the cerebral hemisphere and related disorders. *Radiographics*. <https://doi.org/10.1148/rg.2017160061>.
- Thompson, A.J., Banwell, B.L., Barkhof, F., Carroll, W.M., Coetzee, T., Comi, G., Correale, J., Fazekas, F., Filippi, M., Freedman, M.S., Fujihara, K., Galetta, S.L., Hartung, H.P., Kappos, L., Lublin, F.D., Marrie, R.A., Miller, A.E., Miller, D.H., Montalban, X., Mowry, E.M., Sorensen, P.S., Tintoré, M., Traboulsee, A.L., Trojano, M., Uitdehaag, B.M.J., Vukusic, S., Waubant, E., Weinschenker, B.G., Reingold, S.C., Cohen, J.A., 2018. Diagnosis of multiple sclerosis: 2017 revisions of the McDonald criteria. *Lancet Neurol.* 17, 162–173. [https://doi.org/10.1016/S1474-4422\(17\)30470-2](https://doi.org/10.1016/S1474-4422(17)30470-2).
- Tong, K.A., Ashwal, S., Holshouser, B.A., Nickerson, J.P., Wall, C.J., Shutter, L.A., Osterdock, R.J., Haacke, E.M., Kido, D., 2004. Diffuse axonal injury in children: clinical correlation with hemorrhagic lesions. *Ann. Neurol.* 56, 36–50. <https://doi.org/10.1002/ana.20123>.
- Tong, K.A., Ashwal, S., Holshouser, B.A., Shutter, L.A., Herigault, G., Haacke, E.M., Kido, D.K., 2003. Hemorrhagic shearing lesions in children and adolescents with posttraumatic diffuse axonal injury: improved detection and initial results. *Radiology* 227, 332–339. <https://doi.org/10.1148/radiol.2272020176>.
- Umino, M., Maeda, M., Matsushima, N., Matsuura, K., Yamada, T., Sakuma, H., 2014. High-signal-intensity abnormalities evaluated by 3D fluid-attenuated inversion recovery imaging within the drainage territory of developmental venous anomalies identified by susceptibility-weighted imaging at 3 T. *Jpn J. Radiol.* <https://doi.org/10.1007/s11604-014-0322-0>.
- van Zijl, P.C., Eleff, S.M., Ulatowski, J.A., Oja, J.M., Uluğ, A.M., Traystman, R.J., Kauppinen, R.A., 1998. Quantitative assessment of blood flow, blood volume and blood oxygenation effects in functional magnetic resonance imaging. *Nat. Med.* 4, 159–167. <https://doi.org/10.1038/nm0298-159>.
- Vellinga, M.M., Geurts, J.J.G., Rostrup, E., Uitdehaag, B.M.J., Polman, C.H., Barkhof, F., Vrenken, H., 2009. Clinical correlations of brain lesion distribution in multiple sclerosis. *J. Magn. Reson. Imaging JMRI* 29, 768–773. <https://doi.org/10.1002/jmri.21679>.
- Wardlaw, J.M., Smith, C., Dichgans, M., 2013. Mechanisms of sporadic cerebral small vessel disease: insights from neuroimaging. *Lancet Neurol.* 12, 483–497. [https://doi.org/10.1016/S1474-4422\(13\)70060-7](https://doi.org/10.1016/S1474-4422(13)70060-7).
- Wycliffe, N.D., Choe, J., Holshouser, B., Oyoyo, U.E., Haacke, E.M., Kido, D.K., 2004. Reliability in detection of hemorrhage in acute stroke by a new three-dimensional gradient recalled echo susceptibility-weighted imaging technique compared to computed tomography: a retrospective study. *J. Magn. Reson. Imaging JMRI* 20, 372–377. <https://doi.org/10.1002/jmri.20130>.
- Yanagisawa, M., Kurihara, H., Kimura, S., Tomobe, Y., Kobayashi, M., Mitsui, Y., Yazaki, Y., Goto, K., Masaki, T., 1988. *Nature* 332, 411–415. <https://doi.org/10.1038/332411a0>.
- Wang, Zhou, Bovik, A.C., Sheikh, H.R., Simoncelli, E.P., 2004. Image quality assessment: from error visibility to structural similarity. *IEEE Trans. Image Process.* 13, 600–612. <https://doi.org/10.1109/tip.2003.819861>.